Linking Anatomical and Physiological Properties of Hippocampal Pyramidal Neurons

Dissertation

zur Erlangung des Grades eines
Doktors der Naturwissenschaften

der Mathematisch-Naturwissenschaftlichen Fakultät
und
der Medizinischen Fakultät
der Eberhard-Karls-Universität Tübingen

vorgelegt
von

Lingjun Ding
aus Yangzhou, China

2022

Tag der mündlichen Prüfung: 09.01.2023

Dekan der Math.-Nat. Fakultät: Prof. Dr. Thilo Stehle
Dekan der Medizinischen Fakultät: Prof. Dr. Bernd Pichler

1. Berichterstatter: Prof. Dr. Andrea Burgalossi

2. Berichterstatter: Prof. Dr. Jan Benda

Prüfungskommission: Prof. Dr. Andrea Burgalossi

Prof. Dr. Jan Benda

Prof. Dr. Olga Garaschuk

Prof. Dr. Cornelius Schwarz

Erklärung / Declaration:

Ich erkläre, dass ich die zur Promotion eingereichte Arbeit mit dem Titel:

„ Linking Anatomical and Physiological Properties of Hippocampal Pyramidal Neurons “

selbständig verfasst, nur die angegebenen Quellen und Hilfsmittel benutzt und wörtlich oder inhaltlich übernommene Stellen als solche gekennzeichnet habe. Ich versichere an Eides statt, dass diese Angaben wahr sind und dass ich nichts verschwiegen habe. Mir ist bekannt, dass die falsche Abgabe einer Versicherung an Eides statt mit Freiheitsstrafe bis zu drei Jahren oder mit Geldstrafe bestraft wird.

I hereby declare that I have produced the work entitled "Linking Anatomical and Physiological Properties of Hippocampal Pyramidal Neurons", submitted for the award of a doctorate, on my own (without external help), have used only the sources and aids indicated and have marked passages included from other works, whether verbatim or in content, as such. I swear upon oath that these statements are true and that I have not concealed anything. I am aware that making a false declaration under oath is punishable by a term of imprisonment of up to three years or by a fine.

Tübingen, den ....

Datum / Date Unterschrift /Signature

TABLE OF CONTENTS

Abstract

The hippocampus is of interest to a broad range of neuroscientists, who examine its structure, function, and dysfunction in various pathologies and disorders. Great effort has been put into classifying hippocampal neurons according to their morphological, molecular, and functional characteristics; however, the question of whether and how in vivo neural activity relates to principal cell heterogeneity during natural behaviour has remained unresolved. This study aimed at resolving structure-function relationships in the mouse dorsal hippocampus by investigating three dimensions of principal cell heterogeneity. First, we juxtacellularly recorded and labelled CA2/CA3 pyramidal neurons in freely-moving mice, thus linking quantitative features of dendritic architecture and anatomical position to in vivo activities. We found that a higher proportion of distal dendritic length correlated with higher burst propensity, indicating that entorhinal inputs may determine the burst-firing properties of CA2/CA3 pyramidal neurons. Second, we investigated CA1 principal cell diversity within the deep-superficial axis. We combined the juxtacellular recording technique with optogenetics in freely-moving animals. With restricted Channelrhodopsin (ChR2) expression in Calbindin-positive (Calb1+) neurons, we achieved online readout of cell identity via photostimulation, thus improving the sampling efficacy of superficial layer neurons. We found that Calb1+ CA1 pyramidal cells had weaker spatial modulation and contained less spatial information than Calbindin-negative (Calb1-) neurons, pointing to cell identity as a critical determinant for recruitment into the hippocampal spatial map. Lastly, we explored the anatomical determinants for the recruitment of pyramidal neurons by hippocampal sharp-wave ripple events. The axon initial segment location determined two distinct pyramidal cell types. Neurons with axons initiating from dendrites were more recruited into sharp-wave ripples, indicating that excitatory inputs onto axon-carrying dendrites can escape perisomatic inhibition during hippocampal ripples. Collectively, these results indicate that the recruitment of pyramidal neurons into hippocampal neural ensembles critically depends on cell identity and single cell

morphological features.

1. INTRODUCTION

1.1 The hippocampus and the pyramidal layer

Due to its signature anatomy and central location, the hippocampus has been in the spotlight since the beginning of neuroscience research. Among the earliest researchers who studied hippocampal anatomy, Ramon y Cajal is the most famous for his masterpiece drawing of neuronal arborization in the hippocampus. More impressively, Ramon y Cajal made correct primary conclusions about the functional information flow in the hippocampus based solely on the neuroanatomy. The predominantly unidirectional projections were recognized as a key aspect of hippocampal connectivity. In general, major input region to hippocampus is the entorhinal cortex (EC), while the major output region of hippocampus is subiculum through CA1 region. The information flow in the hippocampus consists of two main paths: the direct pathway (temporammotic pathway), where EC layer III neurons direct project to CA1 pyramidal neurons; and the trisynaptic pathway, where neurons in EC layer II projection first reach dentate gyrus (DG) and CA3 via the perforant pathway, the CA3 then projects to CA1 region via Schaffer Collaterals. The "trisynapse" refer to the three synapses in “EC → DG→ CA3→ CA1” connection (**Figure 1**).

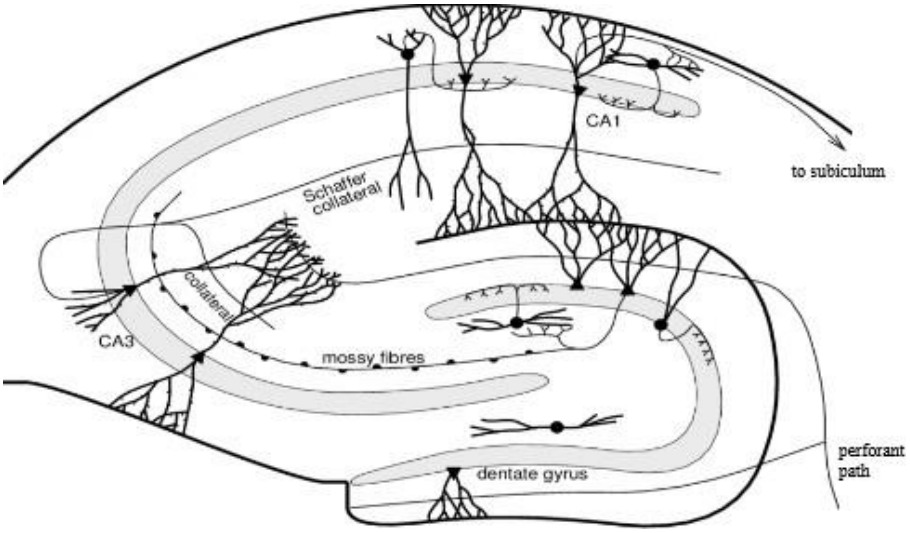

Figure 1. A schematic of information flow in the hippocampal formation.

Information enters the hippocampus from entorhinal cortex via the perforant path. The dentate granule cells make strong projection to CA3 pyramidal neurons via mossy fibers. The CA3 pyramidal cells project recurrently within CA3, and to CA1 via Schaffer collaterals. Information leaves the hippocampus mainly through the path from CA1 and to the subiculum. Adapted from (Schultz et al., 1997).

The pyramidal cells make up the vast majority of the pyramidal layer and are the main principal neurons of the hippocampus. Basically, pyramidal cells in CA1 to CA3 region of the hippocampus have a basal dendritic tree into *stratum oriens* and an apical dendritic tree into *stratum lucidum* (only for CA3 region), s*tratum radiatum* and *stratum lacunosum-molecular*. Although the pyramidal layer of CA1 to CA3 is a continuous structure, dendritic organization and functional circuitry marks the subdivision of the region (**Figure 2**).

CA3 region lays on the proximal end (close to dentate gyrus) of the hippocampal proper. Dendritic organization of the pyramidal cells varies systematically along the transverse axis (proximal to distal); thus, CA3 can be further divided into subregions of CA3a,b,c regions. The CA3 pyramidal cells receive projection from granule cells of DG via mossy fiber. Mossy fiber projection forms the unique structure stratum lucidum in CA3. CA2 was originally defined by Lorente de Nó (1934) as just a transitional region between CA1 and CA3. CA2 pyramidal cells have larger soma and park more

loosely like CA3 pyramidal cells, but they lack the character thorny exercises of CA3 pyramidal cells. Current studies show more unique anatomical and functional features of this region (Hitti & Siegelbaum, 2014; Wintzer et al., 2014). CA1 lays on the distal end of the hippocampal formation with tightly packed smaller soma pyramidal cells, and the dendritic organizations are more homogenous than CA3.

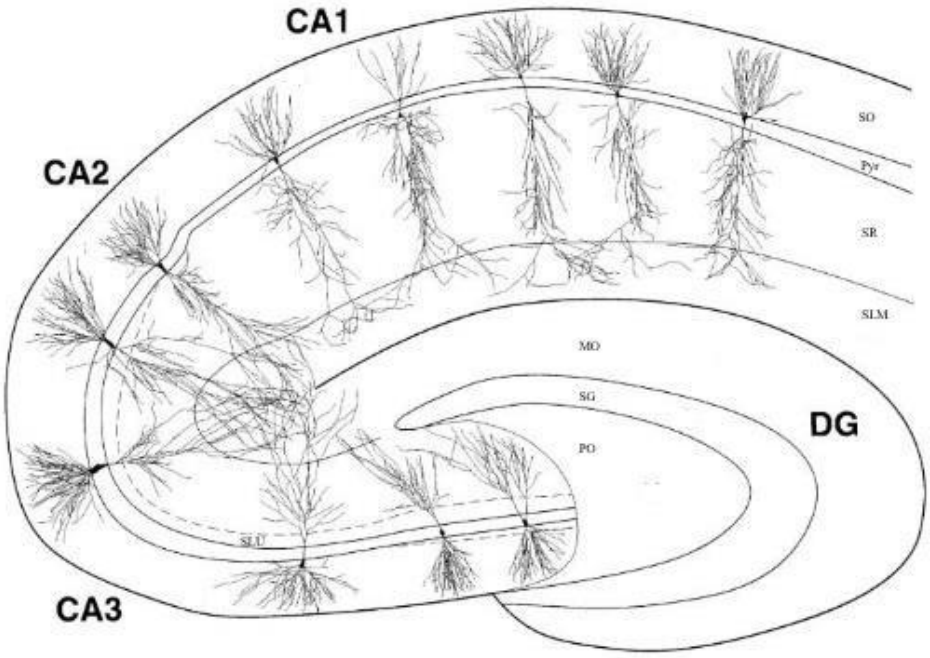

Figure 2 Summary illustration of dendritic morphology of hippocampal pyramidal neurons.

All hippocampal pyramidal neurons display a basal and an apical dendritic tree, note the morphological heterogeneity among and within the neurons of CA1, CA2 and CA3 regions. DG, dentate gyrus; SLU, *stratum lucidum*; SO, *stratum oriens*; Pyr, *stratum pyramidale*; SR, *stratum radiatum*; SLM, *stratum lacunosum moleculare*; MO, molecular layer of DG; SG, granule cell layer of DG; PO, polymorph layer of DG.

Adapted from (Ishizuka et al., 1995)

Unique features of the hippocampus attracted researchers for decades: the single cell layer with strictly laminated inputs, the highly plastic synapses, the unidirectional connection from and to cortical regions, and long surviving slices in vitro, making the hippocampus an idea region to study with slice physiology methods. Recording in acute brain slices can record synaptic and cellular activities as well as field potentials,

providing information on many aspects of the neurons, from membrane properties, cell connectivity to local circuit interactions. As a result, many important features of the hippocampus were found and a lot of these findings led to the establishment of general principles in neuroscience (Andersen et al., 1964; Kandel et al., 1961; Kramis et al., 1975; Vanderwolf, 1969). Further study advanced forward to functional dissection of the hippocampus taking advantage of the comprehensively examined anatomical organization and cellular features in this region.

It is well-accepted now that the hippocampus plays an essential role in memory. Evidence emerged from clinical observations, and milestone evidence is the famous patient H.M. In his case, after surgical removal of the medial temporal lobes, he suffered from amnesia, both anterograde and retrograde. He failed to form new memory about things or episodic experiences, and he lost memory of some years before the operation. Following lesion experiments in animals (Correll & Scoville, 1967; Douglas & Isaacson, 1964; Kaada et al., 1961; Kimble, 1963; Orbach et al., 1960) supported that hippocampal formation is crucial in memory forming and retrieving. Another milestone for hippocampus functional studies is the discovery of place cells, leading to the finding of spatial representation in the brain.

1.2 Place cells and spatial representations in the hippocampus

The first place cell was reported in 1971 (O'Keefe & Dostrovsky, 1971); since then, research about place cells and spatial representation has thrived to unveil the cognitive function of spatial mapping in the brain.

Place cells show spatial localized firing patterns in a specific environment, and different cells have different spatial receptive fields (place fields). The place fields of population spread over the entire environment. Based on these observations, O'keefe and Nadel suggested the idea that the hippocampus serves as a cognitive map while the place cell is the fundamental element of this internal map in their famous book *Hippocampus as a Cognitive Map* (O'keefe & Nadel, 1979).

Spatial representation is normally categorized in three different ways according to

its reference frames: the egocentric, the allocentric and the idiothetic presentation. The egocentric representation means the space is defined concerning an individual's self-position, the allocentric representation means the space is defined to the external world, and the idiothetic representation means the space is defined in relation to an arbitrary point of the environment. The spatial localized firing pattern of place cells makes them an allocentric landmark of the space, as suggested in *Hippocampus as a Cognitive Map*. However, closer examination of place cells showed that sometimes they do not serve as faithful landmarks of the space as they may change their firing patterns in the same environment.

Place cells can change their firing pattern in a short time or over a more extended period, a phenomenon known as place cell remapping. The activity of a group place cells is referred as place cell ensemble. Upon changes in the environment, the place cell ensembles typically change accordingly. Three different types of remapping are reported in the literature: global remapping, partial remapping, and rate remapping. (1) Global remapping happens generally when the location or major cue of the environment changes, the place cell ensembles would change place fields completely (Fyhn et al., 2007; Hayman et al., 2003; Leutgeb et al., 2005; Wills et al., 2005). (2) Partial remapping refers to the phenomenon which change of firing pattern only happens partially in the cell ensemble. When some features of the environment change, e.g., cues in the laboratory environment, some place cells change their firing pattern, but others remain unchanged (Anderson & Jeffery, 2003). (3) Remapping can happen even without changing the position of the place fields. In some researches, the animal performed different tasks in the same environment; the place cells largely remain their place fields, but the in-field firing rates change. This phenomenon is called rate remapping (Frank et al., 2000; Fyhn et al., 2007; Wood et al., 2000).

Combining different remapping strategies allows the animal to quickly adapt its internal presentation of its position in the space to the swiftly changing nature conditions. Different remapping mechanisms are adopted depending on the changes in the environment also on the region of the hippocampus. There are prominent

differences between the CA1 and CA3 regions. For example, when recorded with highly controlled laboratory conditions, the CA3 cells tend to rotate coherently following the proximal cue, while the CA1 cell ensemble does not follow either the proximal or distal cues. When exposed to two completely different environments, the CA3 normally remaps globally while partial CA1 cell ensemble remains (Lee et al., 2004). The local connectivity difference can partially explain the difference in remapping strategies as CA3 region has dominant recurrent connections while the CA1 hardly projects locally. It suggests that different hippocampus regions contribute to different processing pathways of spatial presentation.

1.3 The transverse (proximal-distal) axis of the hippocampal CA2 and CA3 subfields

The transverse axis is considered the principal organization axis in the hippocampus. Studies raised from the observation of heterogeneity of pyramidal cells' dendritic morphologies in rats. Turner and colleagues (Turner et al., 1995) showed a clear difference in the dendritic length and morphology of CA3 cells. Their measurement indicates that the proximal CA3 neurons have shorter total dendritic length and short reach out, resulting in very few dendrites of CA3c region reaching the SLM region. Later studies confirmed that CA3c cells have the shortest apical dendrite and dendrites in SLM. From slice patch-clamp experiments, intrinsic properties of the CA3 cells also display a notable proximal-distal gradient. At the proximal end of CA3, the cells are the easiest to excite with the most negative resting potential, highest input resistance, and lowest sag. The proximal-distal gradient is consistent across the entire dorsal-ventral level of hippocampus and is most evident at the ventral level of hippocampus (Sun et al., 2020; Sun et al., 2017).

Many studies have also reported the gradient change of local and global connectively along the proximal-distal axis. Early in 1994, study showed a pattern of projection gradient of the CA3 pyramidal cells: the proximal CA3 cells projection

predominantly terminates on the apical dendrites of both CA1 and CA3 cells while the CA3 distal cells innervate more on the basal dendrites of CA1 and CA3 cells (Li et al., 1994). It was later showed that the mossy fiber input strength decreases from proximal to distal CA3 while the cortical input increase in the meantime (Sun et al., 2017). Li and colleagues also noted that the axon collaterals of a CA3 neuron remain in the subfield of this cell, providing structural support for later findings of functional segregation of the CA3 region (Li et al., 1994). Interestingly, recording in brain slices showed that the strength of recurrent excitation of CA3 subregion did not follow a similar simple gradient (Sun et al., 2017).

Studies moved on to reveal the functional difference among the subfields of CA3. Hippocampus is known for high involvement in spatial representation and memory forming; different studies indicate functional segregation in both aspects.

A lesion in the DG region leads to the animals losing their ability to distinguish a novel environment or changes in their familiar environment. While CA3a,b lesions showed no sign of this kind of deficit, the lesion on the CA3c, interestingly, showed intermediate deficits. The results of this study suggested a gradient of functional involvement in memory of the DG-CA3 circuit (Hunsaker et al., 2008). Early immediate gene (e.g., Arc, cFos) expression indicates the activation of a certain cell population. Studies of Arc expression have shown differential involvement of CA3 subregions depending on the performed tasks. For example, CA3b is the most strongly activated region during fear memory retrieval (Sun et al., 2017), while proximal CA3 (CA3c) is more active during a "non-spatial delayed nonmatching-to-sample recognition memory task" or "conditions of partial cue change tasks" (Marrone et al., 2014; Nakamura et al., 2013). Interestingly, a similar gradient of function in CA1 has also been reported: a trend of more recruitment of distal CA1 cells in similar tasks is consistent with the projection topography as proximal CA3 preferably projects to distal CA1 while distal CA3 projects more to proximal CA1(Henriksen et al., 2010; Nakamura et al., 2013). These findings indicate that functional segregation in CA3 contributes to information flow in the entire hippocampus.

The proximal end of CA3 is believed to be more recruited in spatial representation because they carry higher spatial information, and the place cells here have sharper place fields. Proximal and distal populations tend to use different mechanisms in response to local and distal cue changes. In general, the proximal CA3 tends to remap globally, and this tendency decrease along the CA3-CA2 axis (Lee et al., 2015; Lu et al., 2015). It is normally assumed that the dentate gyrus operates the pattern separation function while the CA3 performs pattern completion (Leutgeb et al., 2007). Pattern separation was suggested initially as "Expansion Coding" by Marr (Marr, 1969). In his hypothesis, DG receives inputs from EC with minor differences that represent different environments, and it will separate them by recruiting a small ensemble of cells in each different environment so that the representation of the space is very different in the brain. In the meanwhile, the downstream CA3 region performs the pattern completion function, as also suggested by Marr as "Collateral Effect". It works so that when the inputs have small variables, the system still completes the coding to an already existing pattern via the highly recurrent circuitry in CA3. Pattern completion is helpful when only a small fraction of the environment has changed, and the animal can still recognize the place. A new study challenged the idea that the CA3 function homogeneously in pattern completion. It was shown that the proximal part of CA3 (CA3c region) works more similarly to DG to perform pattern separation while the pattern completion is performed more in media and distal CA3 (Lee et al., 2004).

In summary, studies on the heterogeneity of CA3 principal cells along the transverse axis merged and agreed that the CA3 consists of functionally segregated subregions.

CA2 is a small region (about 200μm width in the coronal section of mouse brain) between CA1 and CA3. This region was overlooked for decades because of its small size and unclear anatomical border. CA2 has long been assumed to be just a transition region of CA3 to CA1 (Lein et al., 2005). However, recent studies have shown its unique cell profile and functions (Dudek et al., 2016; Lein et al., 2005). Unlike the neighbouring CA1 and CA3 regions, the CA2 region is unstable in spatial

representation over time even in the same environment, indicating its different role in spatial mapping (Mankin et al., 2015; Wintzer et al., 2014). Indeed, inactivating the CA2 region did not impair the retrieval of spatial memory of the mouse, but it significantly impaired the forming of social memory (Hitti & Siegelbaum, 2014; Oliva et al., 2020).

PCP4, RGS14, and Amigo are the most used biochemical markers for CA2. The proximal end of CA2 was before defined as the end of dentate mossy fiber because it was believed that mossy fiber does not make synapses onto CA2 cells. It was proved to be not the case by Kohara and colleges (Kohara et al., 2014). They showed that dentate gyrus makes functional projection to CA2 through mossy fiber. This projection has similar synaptic facilitation and feed-forward inhibition properties like the classical mossy fiber connection on CA3. In a following study, the authors defined the end of mossy fiber as the mid-point of CA2 and divided CA2 into proximal and distal parts (Fernandez-Lamo et al., 2019). They found that proximal CA2 receives stronger input from DG and CA3, while distal CA2 is more influenced by EC input. During theta LFP oscillations when animal runs or sleeps in REM phase, local phase of proximal CA2 is more similar to CA3, and distal CA2 is more similar to CA1 neurons. Heterogeneity among CA2 cells can also be found regarding gamma oscillation coupling and spatial representation (Fernandez-Lamo et al., 2019). Taken together, connectivity and function diversity can be found even in the small CA2 region.

1.4 The radial (deep-superficial) axis of the CA1 subfield

Among the principal cells of the hippocampus, CA1 pyramidal cells were probably studied most extensively. The proximal-distal topography of cell morphology and physiology feature of CA1 pyramidal cells were exhaustively described. However, fewer studies were performed to explore the radial (deep-superficial) axis of CA1. Along this axis, pyramidal cells can be separated into two populations by immune markers, such as Calbindin and Zinc (Slomianka et al., 2011).

During the development of the hippocampus, neuron migration follows an inside-

out manner like the neocortex: the deep layer consists of early-developed neurons, while the superficial layer consists of late-born neurons. That is also true for the pyramidal neuron of CA1. In CA1 *strata pyramidal*, the superficial layer consists of the late born cells that are positive for both Calbindin and Zinc. Calbindin and Zinc were reported to be involved in synaptic plasticity (Slomianka et al., 2011), indicating different roles of deep and superficial CA1 neurons in memory processing and proceeding.

Variations in morphology and connectivity between deep and superficial CA1 neurons were also reported in several literatures (Kohara et al., 2014; Li et al., 2017; Masurkar et al., 2017; Masurkar et al., 2020). The apical dendrites of superficial Calb1+ cells are more complex and tend to branch close to the soma. However, no evidence showed the difference in the total length of the apical dendrites and apical tuft. Branching characteristics of the dendrite may affect the potential propagation in the neuron, thus gating the information flow (Andersen, 1960; Andersen et al., 1964; Cragg & Hamlyn, 1955; Fujita & Sakata, 1962). Indeed, it has been shown that CA1 cell dendrites can have active dendritic spikes.

Connectivity-wise, studies have shown slightly controversial projection patterns of CA1 deep and superficial pyramidal cells. However, they arrived at a similar point: there are connectivity distinctions along the radial axis of this long-considered homogeneous laminar structure. Li and colleagues showed that MEC projects to both deep and superficial CA1 pyramidal cells universally; meanwhile, LEC projects preferentially to superficial cells (Li et al., 2017). Patch-clamp data in slice physiology also showed slightly differential projection patterns from MEC and LEC regions (Masurkar et al., 2017). More specifically, they described that LEC projects to superficial CA1 pyramidal cells towards the distal end while the MEC projects to deeper CA1 pyramidal cells towards the proximal, adding one more dimension of complexity to this long-believed anatomical simple region. EC is the entry point for cortical information to the hippocampus, and LEC and MEC are considered to carry the "What" and "Where" information respectively. The projection preference of EC

subregions to CA1 leads to the hypothesis that deep and superficial sublayers of CA1 process differently in contexture or episodically memory. Indeed, it was further showed that the projection of LEC to CA1-deep cells is directly involved in the olfactory learning process (Li et al., 2017).

Kohara et al.'s study showed a preferential CA2 projection to deep CA1 pyramidal cells and a direct projection to CA2 from DG, therefore creating a side path of DG-CA2-CA1 information flow in addition to the classical trisynaptic connection (Kohara et al., 2014). They proposed that this side path would prevent overlearning in the classical DG-CA3-CA2 pathway. Besides connection from other principal cells, studies also showed projection preference of local interneuron of CA1 region (Lee et al., 2014). They showed that the deep cells receive more inhibition from local Parvalbumin interneurons (PV+) interneurons while the superficial cells are more likely to excite PV+ interneurons; thus, the superficial cells can preferentially provide feed-forward inhibition to deep cells, suggesting that the CA1 deep cells may shape the overall representation in the hippocampus processing flow.

The morphology and connectivity diversity between deep and superficial CA1 cells predicted their physiology and function differences. Evidence emerged from various experimental approaches showing their divergence in firing properties (firing rate, firing burstiness, polarity during oscillation) and spatial representation. Studies using multichannel electrodes (tetrodes or silicon probe) or Ca2+ imaging showed that the cells of the deeper layer are overall more active, for their higher firing rate and higher tendency to fire in bursts than superficial cells. Studies also showed that place cells in the deep layer have an overall faster dynamic (Mizuseki et al., 2011); they can form and disappear fast when the animal is provided or deprived of a tactile-visual cue. Thus, those cells were named "landmark vector cells" (Danielson et al., 2016; Geiller et al., 2017; Oliva et al., 2016). This kind of cells typically form place fields in the zone with rich tactile or visual cues. On the other hand, place cells from the superficial layer are more stable without anchoring reference in the space; therefore, they are considered to present contexture information. Other than the preferential recruitment in different

environments, CA1 place cells seem to use distinct strategies to encode place: deep place cells prefer to use phase code, while superficial place cells prefer to use rate code in the place field (Fattahi et al., 2018; Sharif et al., 2021).

Merging evidence clearly suggests a separation of CA1 cells of deep and superficial layers in their identity and function. However, limited by the methods, researcher can only separate the recordings by the relative depth of the recording site, causing miss-assignment of the cells and loss of data at the transient location. Further studies can be carried out to fill this gap.

1.5 Methodological developments in recording neuronal activities in freely moving animals

Recording neuronal activities during animal natural behavior is challenging and rewarding. The pioneer recordings of single-cell activities in the hippocampus of awake, behaving animals discovered place cells (O'Keefe & Dostrovsky, 1971). Since then, hippocampal research benefitted greatly from methodology developments and in turn requested more delicate and inventive techniques.

Early recordings in freely moving animals were performed with single or pair of single-channel electrodes to record single-cell extracellular activities. Soon after the discovery of place cells, scientists proposed that the hippocampal neurons encode space in ensembles (O'keefe & Nadel, 1979); thus, further research required new techniques to enable simultaneous recording of a larger number of neurons. This was achieved by bundling a few electrodes (most common with four electrodes forming a tetrode). Each cell's activity is separated by its constant waveform picked up by different electrodes, a process called spike sorting. A huge amount of great discovery was performed with this technique (Csicsvari et al., 1999; Gray et al., 1995; Henze et al., 2000; Holmgren et al., 2003).

Two main paths can be drawn in the subsequent development of in vivo electrophysiology methods. The first one is to increase the simultaneous sampling size

of neurons. Various structures of electrodes and electrode arrays have been put to use. Hundreds, even thousands of neurons' simultaneous activities were recorded. The structure can be formed by either a single electrode as Tungsten or multiple site electrodes like tetrodes and silicon probes which contain multiple recording sites along the shank, giving higher and higher spatial precision of the recorded regions. Furthermore, recent studies with miniaturized two-photon microscope or fiberscope achieved large-scale calcium imaging of neural activity during animal natural behaviour (Szabo et al., 2014; Zong et al., 2022; Zong et al., 2017).

This path of methodology development leads to a massive dataset of neuronal activity ensembles. Scientists aim to decipher the mechanism of information coding in the brain from these data.

Meanwhile, the other path aims to acquire more aspects of the neurons in addition to its electrical potential discharges in natural behaviour. Indeed, combined with optogenetic and/or transgenic animal tools, partial information of the recorded neurons can be obtained with large-scale recording techniques discussed before. However, single-cell morphology is still out of reach for these methods. It is well accepted that cell morphology highly correlates to its activity and function; however, resolving the structural correlates in natural behaving conditions is still a methodological challenge. In vivo patch clamp can achieve this goal, but the procedure is technically challenging even in relatively stable conditions. The patch-clamp-like juxtacellular recording technique drastically decreased the difficulty of obtaining single-cell recordings while maintaining the possibility of injecting a dye into the cell with electrotophy (Pinault, 1994, 1996). Juxtacellular recording can also be adapted to record and label single neurons in freely moving rats and mice. Although losing the possibility of recording under-threshold activities and potential manipulation in patch clamp configuration, the juxtacellular recording technique provides a high signal-to-noise ratio that leads to a "ground-truth" level of single-cell activity. Furthermore, evoking spikes of the recorded neuron can be achieved either by current injection or optogenetic techniques in the juxtacellular configuration.

1.6 Aim of the study

We aimed at resolving structure-function relationships in hippocampal pyramidal neurons. We investigated three dimensions of the principal cell heterogeneity. First, we explored the CA2/CA3 morphological and physiological properties along the transverse axis. We quantitatively analysed dendritic morphological features and anatomical position, and linked them to in vivo activity profiles. Second, we explored pyramidal cell heterogeneity within the CA1 region. We advanced our technique to improve the sampling efficacy of superficial layer neurons by combining juxtacellular recordings with optogenetic tagging. Lastly, we used the juxtacellular recording and labelling technique to explore anatomical determinants for neuronal recruitment into sharp-wave ripple events.

2. MATERIELS AND METHODS

2.1 Experimental subjects

Wild-type C57BL/6J mice (RRID:IMSR_JAX:000664; male, >8 weeks old; Charles River) and Calb1^{cre} mice (RRID:IMSR_JAX:028532; male, >8 weeks old; The Jackson Laboratory) were used in this study. All experimental procedures were performed according to German guidelines on animal welfare under the supervision of local ethics committees.

2.2 Behaviour trainings

Animals used in awake head-fixed recording were implanted with a metal post, and a recording chamber under ketamine/xylazine anaesthesia. Animals used in freely-moving experiments were implanted additionally with a 10-pins connector for connecting the miniaturized headstage.

Animals used in both awake head-fixed and freely-moving recordings were habituated to head-fixation. After recovery from the surgery (at least 2-3 days), the animals were progressively familiarized to the experimenter and the restrainer box, and then trained for head-fixation. The animals were head-fixed by securing the head-post to the head-post holder in the restrainer box. The first fixation should not last more than 10-30 s. Slowly extend the fixation time over a number of days, until the animal can sit quietly under head-fixation − i.e. without struggling and/or displaying overt behavioural signs of stress − for a minimal period of 15 min.

Animal used in freely-moving experiments were further trained to perform pellet chasing task in the recording arena. From the second/third session of head-fixation trainings onwards, upon release from fixation, the mouse was placed in the behavioural arena, where the food pellet reward is provided. A dummy headstage with LEDs were connected to the connector implanted on the mouse head to habituate the animal to the final recording configuration.

2.3 Viral injection

Viral constructs used in this study consist: AAV-CAG-flex-GFP (Cat#BA-002, Charitè Viral Vector Core, Berlin, Germany; RRID:Addgene_28304) and AAV-EF1a-flex-ChR2-eYFP (Addgene, Cat#20298-AAV9, Watertown, MA; RRID:Addgene_20298) for visualizing CA1 Calb1+ neurons; AAV-hSyn1-flex-ChR2(H134R)-mCherry (Cat#v332-1, Viral Vector Facility, University of Zürich, Zurich, Switzerland; RRID:Addgene_20297), AAV-hSyn1-flex-oChIEF-TdTomato (Charitè Viral Vector Core, Cat#BA-030; RRID:Addgene_30541) to selectively express ChR2 or oChIEF in CA1 Calb1+ pyramidal neurons and DG granule cells; AAV-CAG-ChR2-mCherry (Addgene, Cat#100054; RRID:Addgene_100054) to express ChR2 in CA3 neurons.

Viral injections were performed via pressure injection, animals were anesthetized with fentanyl-midazolam-medetomidine anaesthesia (Burgalossi et al., 2011; Chakrabarti and Schwarz, 2018). A pression-injection pump assembly (Microinjection Syringe Pump, Cat#UMP3T, WPI) was mounted onto a Robot Stereotaxic (StereoDrive, Cat#9001001 Neurostar) or onto a conventional micromanipulator (LN Junior Unit, Luigs and Neumann). Viral vector solution (100-150 nL) was injected at a flow of 10-15 nL / min (typically, 10 min injection time).

Typical expression time of the viral vectors was twelve to eighteen days. After that mice were subjected to histological analysis (see details in **2.8 Immunohistochemistry and neural reconstruction**) or electrophysiological recordings (see details in **2.4 Juxtacellular recordings** and **2.5 Opto-tagging**).

In Calb1^{cre} mice injected with flex-ChR2 or flex-oChIEF constructs, depolarization opsin was exclusively expressed in Calb1+ neurons. In CA1 region, 0 out of 272 neurons were ChR2-positive/Calb1-negative, thus confirming the specificity of the Calb1^{cre} driver line (Daigle et al., 2018; Nigro et al., 2018). Viral titers and injection volumes were optimized to obtain high infection efficiency and ChR2 expression levels (~95.8% of Calb1-positive neurons were also ChR2-positive; 261/272 neurons),

thereby minimizing the occurrence of false negatives in our opto-tagging experiments.

2.4 Juxtacellular recordings

Juxtacellular recordings were performed in anesthetized, awake head-fixed and freely-moving animals. Animals involved in head-fixed or freely-moving experiments underwent behavioural trainings as described before (**2.2 Behaviour Trainings**).

Mapping experiments were performed in anesthetized or awake animals to precisely estimate the recording location for freely-moving experiments. The target region of this study is the pyramidal layer of the mouse hippocampus. A glass electrode was lowered into craniotomy and the occurrence of sharp-wave ripples complexes, their polarity reversal and the increased juxtacellular hit rates, and depth readout from the manipulator served as reliable electrophysiological signatures for precisely localizing the CA1 or CA3 pyramidal layer.

Mapping experiments were performed with opto-patcher for opto-tagging freely-moving experiments to evaluate the ChR2 expressing level in opto-tagging experiments as well (see details below in **2.5 Opto-tagging**).

Juxtacellular recordings were performed with glass electrodes with ~2 μm diameter tip and 4-6 mΩ resistance and filled with Ringer's solution containing (in mm): 135 NaCl, 5.4 KCl, 5 HEPES, 1.8 CaCl2, and 1 MgCl2 or intracellular solution containing the following (in mm): 135 K-gluconate, 10 HEPES, 10 Na2-phosphocreatine, 4 KCl, 4 MgATP, and 0.3 Na3GTP. Osmolarity was adjusted to 280-310 mOsm. For experiments aim to obtain the neuronal morphology, 1.5%-2% Neurobiotin (Vector Laboratories) were added in the pipette solution.

For juxtacellular recordings in anesthetized or awake head-fixed animals, the mouse was head-fixed by means of either the stereotaxic frame or the head-post pre-implanted on the head. The glass electrode was lowered into the craniotomy by means of a conventional micromanipulation (LN Junior Unit, Luigs and Neumann) and recorded by the conventional headstage (NPI electronic).

For juxtacellular recordings in freely-moving animals, the glass electrode was

lowered into the brain by a miniaturized micromanipulator (secured onto a custom-made base) and recorded by an ELC miniature headstage (connected to the preimplanted pin-connector), while animals collected food pellets in an O-shaped, linear maze (70 × 50 cm, 9-cm-wide path, 16-cm-high walls, **Figure 3**).

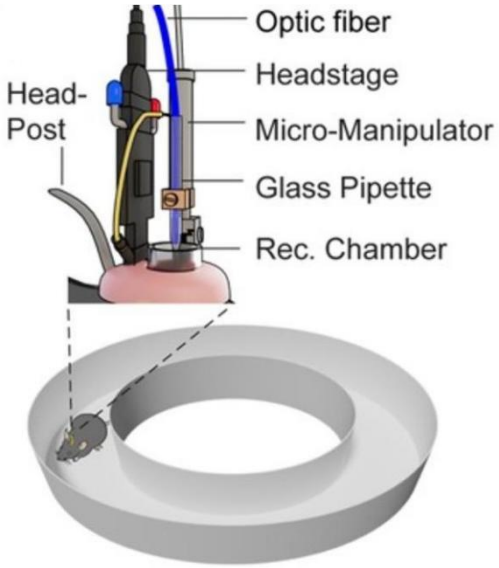

Figure 3 Juxtacellular free-moving recording configuration
A schematic drawing showing the final assembled implant for juxtacellular opto-tagging recording and circular arena. For experiments without opto-tagging procedures, the optic fiber is not included in the assembly.
Adapted from (Ding et al., 2020).

Juxtacellular labelling was performed in subset of experiments aiming to acquire neuronal morphology. Basically, biocytin was injected into the cell by current (typically 5–20 nA square current pulses, 50% duty cycle: 200 ms ON, 200 ms OFF) and monitored by the modulation of the cell's firing rate (i.e., 'entrainment'). During the entrainment procedure, broadening of the spikes and small negative DC shifts in the baseline potential should present. The average duration of the labeling procedure in anesthetized animals is 5-10 min and in awake-head-fixed and freely-moving animals is 1-3 min.

The juxtacellular voltage signal was acquired via conventional or miniaturized headstage, and an ELC-03XS amplifier (NPI Electronic), sampled at 20 kHz by a POWER1401-3 analog-to-digital interface under the control of Spike2 Software

(CED). The location of the animal in freely-moving experiments was tracked using two LEDs (red and blue) glued to the headstage and mounted on the mouse's head during experiments. The LED position was acquired via a video (25 Hz frame rate) with the IC Capture Software (The Imaging Source).

2.5 Opto-tagging procedures

Opto-tagging were performed by inserting an optic fiber (50 μm core) in the glass pipette and fixed by means of the opto-patcher (ref, and source) in head-fixed configuration or a drop of silicon in freely-moving configuration. The optical fiber was connected to a 473 nm laser (Oxxius, Cat#LBX-473–300) and controlled by the Spike2 software. The laser output (controlled by the Oxxius software) was calibrated and measured at the glass electrode tip (containing Ringer solution). Light intensities were adjusted in mapping experiments and on a cell-by-cell basis.

Opto-tagging during juxtacellular recording were performed by delivering short pulses of blue light (1- to 5-ms long pulses, at 1-40 Hz) at the end of the recording session to test for light-evoked spiking activities. For directly light-activated CA1 neurons, low-power intensities were sufficient for eliciting spiking (typically <1 mW; range 0.1–1 mW, see in **Figure 12** and **Figure 13**). For the indirectly activated CA1 and CA3 neurons (**Figure 14, 15**), higher light power (>1 mW; range 1–2.5 mW) was needed for evoking spiking compared to direct light activation.

Peristimulus time histograms (PSTHs) were computed with 0.1 ms bin size (the only exception being the putative Calb1- cell in **Figure 17**, where the PSTH was computed with a bin size of 20 ms for display purposes). Spike latencies to light stimulations were computed by measuring the time from the onset of the light stimulus to the first evoked spike within a 20-ms window. The mean latency for each cell was calculated as the average spike-latency across all trials.

2.6 Analysis of electrophysiology data

Spike signals from juxtacellular voltage traces were manually isolated with the help of principal component analysis via custom-made codes written in MATLAB, as described previously (Burgalossi et al., 2011). Recordings (or portions of recordings) in which cellular damage was observed (e.g., spike-shape broadening, increase in firing rate accompanied by negative DC shifts of the juxtacellular voltage signal, as described in (Herfst et al., 2012; Pinault, 1994, 1996) were excluded from the analysis.

The burst index was used as a measure of bustiness, and defined as in (Hunt et al., 2018; Neunuebel & Knierim, 2012) as the sum of spikes with an ISI < 6 ms, divided by the total number of spikes. The theta index was used as a measure of spiking rhythmicity in the theta frequency range, and it was computed as the average power within 1 Hz of the maximum of the autocorrelation function in the theta band divided by the average power between 1 and 50 Hz (Yartsev et al., 2011). Minimum spike number threshold were applied in each project when calculating neural properties (e.g., burst index, theta index, spatial information, sparsity).

In this study in line with previous work (Diamantaki et al., 2018; Diamantaki, Frey, Berens, et al., 2016; Diamantaki, Frey, Preston-Ferrer, et al., 2016; Epsztein et al., 2011; Lee et al., 2012), a linear circular maze was used for sampling spatial modulation in pyramidal neurons within shorter recording durations compared with extracellular recordings (see **Figure 3**). Recording displayed in **Figure 18** were converted to a one-dimensional representation. This was done by first projecting the X–Y coordinates onto the ellipse that best approximated the trajectory, and then converting the projected coordinates into a one-dimensional representation by finding their associated positions along the linearized ellipse.

For the analysis of spatial firing patterns, a speed threshold was applied (speed >1 cm/s) and only recordings with >50 spikes and ≥3 laps were included.

2.7 Analysis of spatial modulation

The position of the mouse was defined as the midpoint between two head-mounted LEDs. For computing color-coded firing rate maps, only spikes during movement (>1cm/s) were included. Space was discretized into pixels of 2.5 x 2.5 cm, for which the occupancy (z) of a given pixel x was calculated as

$$z(x) = \sum_t w(|x - x_t|)\Delta t$$

where x_t is the position of the mouse at time t, Δt the inter-frame interval, and w a Gaussian smoothing kernel with σ = 0.5 cm. Then, the firing rate (r) was calculated as

$$r(x) = \frac{\sum_i w(|x - x_i|)}{z}$$

where x_i is the position of the mouse when spike i was fired. The firing rate of pixels, whose occupancy (z) was less than 20 ms, was not shown.

The spatial information of a cell in bits per spike is calculated as (Markus et al., 1994)

$$I_{spike} = \sum_n p_n * (\frac{\lambda_n}{\lambda}) * log_2(\frac{\lambda_n}{\lambda}))$$

where p_n is the probability of the animal being in n-th pixel bin, λ_n is the mean firing rate in the n-th pixel bin, and λ is the overall mean fire rate of the cell.

The sparsity of a cell is calculated as (Markus et al., 1994)

$$Sparsity = \sum_n \frac{p_n * \lambda_n^2}{\lambda^2}$$

where p_n is the probability of the animal being in n-th pixel bin, λ_n is the mean firing rate in the n-th pixel bin, and λ is the overall mean fire rate of the cell.

Statistical analysis was performed with standard MATLAB functions. No statistical methods were used to predetermine sample sizes, but our sample size estimates were based upon previous work addressing structure-function relationships of single neurons with similar techniques (Diamantaki et al., 2016; Preston-Ferrer et al., 2016; Tang et al., 2014, 2015).

To assess the statistical significance of spatial modulation, a standard shuffling procedure was used. Specifically, for each trail of the shuffling procedure, spike times were randomly time-shifted within ±10 s window, with shifted spike times exceeding the total duration of a recording being wrapped around to the beginning of the recording. For each permutation, the spatial information was calculated, and the procedure reiterated 1000 times to generate a null distribution for each cell. A cell was defined as place cell when (1) its spatial information exceeded the 95th percentile of its null distribution (i.e., significantly spatially modulated), and (2) at least one place field < 300 pixels was detected. The in-field firing rate was calculated as the average firing rate over all place field pixels. To calculate the size of the place fields, a firing field was considered as at least 40 contiguous pixels with average firing rate exceeding 20% of the peak firing rate (Leutgeb et al., 2007; Neunuebel & Knierim, 2012).

2.8 Immunohistochemistry and neural reconstruction

For histological analysis, animals were euthanized with an overdose of pentobarbital and perfused transcardially with 0.1 M phosphate-buffered saline followed by a 4% paraformaldehyde solution. Brains were sliced on vibratome (VT1200S; Leica, Wetzlar, Germany) to obtain: 70-µm-thick sagittal or coronal sections. Immunostainings were performed on free-floating sections as described previously (Ray et al., 2014). To reveal the morphology of juxtacellularly labeled CA1, CA2 and CA3 cells (i.e., filled with Neurobiotin), brain slices were processed with streptavidin-546 (Thermo Fisher Scientific, Waltham, MA, Cat#S1225) or streptavidin-488 (Thermo Fisher Scientific, Cat#S1223).

Immunohistochemical stainings for PCP4 were performed with the rabbit anti-PCP4 (catalog #HPA005792, Sigma Millipore), as in previous work on hippocampal CA2 (Botcher et al., 2014; Hitti & Siegelbaum, 2014; Kohara et al., 2014). PCP4 expression within the hippocampus was consistent with previous work, with high immunoreactivity being observed in the CA2, granule cell layer, and fasciola cinerea (Kohara et al., 2014; Swanson & Hahn, 2020) as well as scattered expression within

the proximal CA1 and CA3a (Fernandez-Lamo et al., 2019; San Antonio et al., 2014; Swanson & Hahn, 2020).

Immunohistochemical stainings for Calb1 were performed with a rabbit anti-Calbindin antibody (Swant, Cat#300; RRID:AB_10000347). Fluorescence images were acquired by epifluorescence microscopy (Axio imager; Zeiss, Jena, Germany) and confocal microscopy (LSM 900; Zeiss).

For cell reconstruction, after fluorescence images were acquired, the Neurobiotin staining was converted into a dark DAB reaction product followed by Ni2+-DAB enhancement protocol (Klausberger et al., 2003). Neuronal reconstructions were performed manually on DAB-converted specimens with Neurolucida software (MBF Bioscience, Williston, Vermont), and displayed as 2D projections. For the analysis of CA1 pyramidal neuron, dendritic ratio was defined as the total apical dendritic length within the SLM divided by the total apical dendritic length (**Figure 4**).

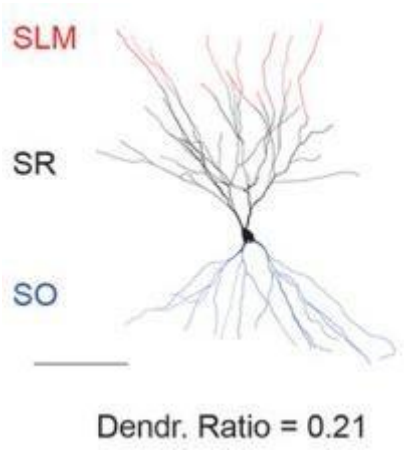

Figure 4 Illustration of dendritic ratio calculation
Dendritic morphology reconstruction of a representative pyramidal neuron, recorded in a freely-moving mouse. Scale bar, 100 µm. Red: dendrites located in SLM; Black: dendrites located in SR; Blue: basal dendrites. The dendrite ratio is calculated as the length of dendrite in SLM (red) divided by total length of apical dendrites (red and black). The dendritic ratio of the representative neuron is indicated.
Adapted from (Ding et al., 2020).

2.9 Statistical analysis

The sample size estimates were based on previous work addressing structure-

function relationships of single neurons with similar techniques (Diamantaki, Frey, Berens, et al., 2016; Preston-Ferrer et al., 2016; Tang et al., 2014). The sample size of individual projects is similar to those reported in previous publications. Neuronal reconstructions and morphologic analysis were performed blind to the electrophysiological data. Statistical analysis was performed with MATLAB.

For linear regressions, adjusted coefficients of determination (R^2) are reported. Statistical significance was assessed by a two-sided Wilcoxon rank-sum test with 95% confidence intervals (Holm-Bonferroni correction for multiple comparisons). Data are presented as mean ± Standard Deviation (SD), unless indicated otherwise.

3. RESULTS

3.1 Structural correlates of spatiotemporal firing properties in CA2 and CA3 pyramidal neurons.

To explore structure-function relationships in the CA2 and CA3 regions of the dorsal hippocampus, we juxtacellularly recorded single cells activities in freely moving mice. Altogether, 174 single-cell recordings were assigned to CA2/CA3 region according to either post hoc histological confirmation or local field potential features (**Figure 5**). Pyramidal neurons (n =140) and fast-spiking interneuron (n = 19) were separated according to standard electrophysiological criteria, i.e. thresholds of 0.4 ms action potential Peak-to-Trough time and 10 Hz average firing rate (Fox & Ranck, 1981; Preston-Ferrer et al., 2016; Sik et al., 1995). A subset of the recorded neurons were labelled with Neurobiotin (see also **Figure 6**). Identified pyramidal neurons and interneurons displayed signature morphologic features (Figure 6): the pyramidal neurons showed typical apical and basal dendritic trees, while on other hand the interneuron had more localized dendritic trees and dense axonal plexus. All identified pyramidal neurons and interneurons were consistent with the electrophysiology classification criteria (**Figure 5**).

Putative interneurons (classified by the thresholds of Peak-to-Trough times and average firing rates) displayed significantly higher firing rates and narrower spike waveforms than pyramidal cells (average firing rates: Pyr, 2.16±2.12 Hz; FS, 52.97± 25.02 Hz; p=1.11e-24, **see Figure 5, Figure 6 and Figure 7a**). As expected, interneurons in CA2/CA3 region carried low spatial information (Pyr, 1.94±1.63 bits; FS, 0.01±0.04 bits; p=3.27e-17, **Figure 7B**). Interestingly however, they showed low theta oscillation locking activities (Pyr, 3.90±2.49; FS, 2.97±3.34; p= 0.018, **Figure 7C),** unlike classical CA1 fast-spiking interneurons (Ranck Jr, 1973).

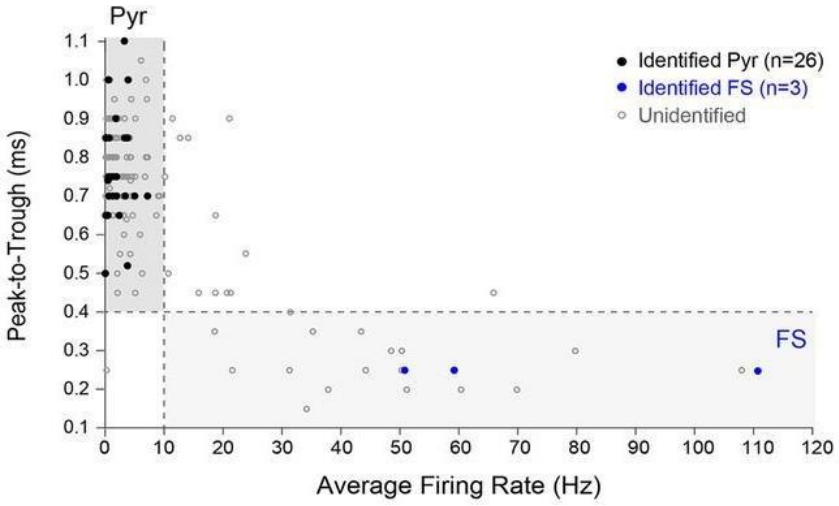

Figure 5 Juxtacellular recordings of CA2 and CA3 neurons in freely-moving mice.

Scatterplot showing the distribution of action potential peak-to-trough times and average firing rates for all active neurons recorded in freely-moving mice (n = 174). Black dots show the distribution identified Pyramidal cells (Pyr, n = 26). Blue dots represent identified fast-spiking interneurons (FS, n = 3). Gray circles represent nonidentified recordings (n = 145). The thresholds of 0.4 ms Peak-to-Trough times and 10 Hz average firing rate for classifying pyramidal cells and fast-spiking interneurons indicated by the dotted lines.
Adapted from (Ding et al., 2020).

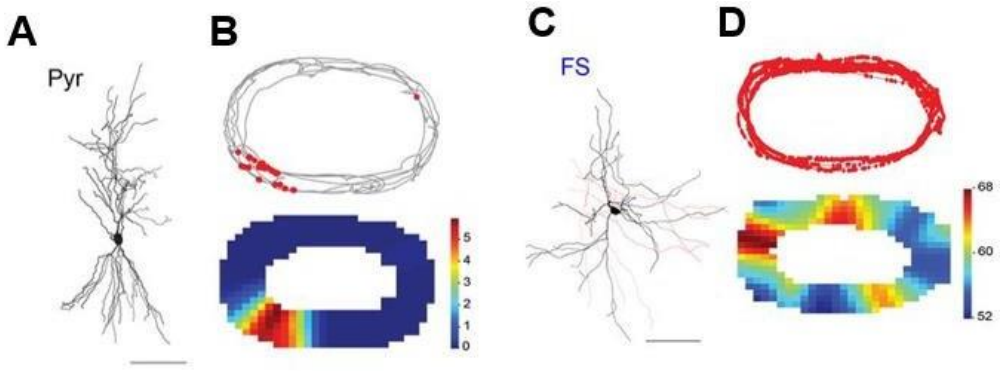

Figure 6 Representative identified pyramidal neuron and interneuron recorded in CA2 and CA3 region in freely-moving mice

(A) Dendritic morphology reconstruction of a representative CA2 Pyramidal neuron (Pyr). Scale bar, 100 μm.
(B) Spike-trajectory plot (top) and color-coded rate map (bottom) for the neuron shown in A. Red dots represent action potentials. The color bar indicates firing rate (Hz).
(C) Dendritic (black) and partial local axonal (red) morphology reconstruction of an identified fast-spiking interneuron (FS), located in CA3a Pyramidal layer. Scale bar, 100 μm.
(D) Spike-trajectory plot (top) and color-coded rate map (bottom) for the interneuron shown in C.
Adapted from (Ding et al., 2020).

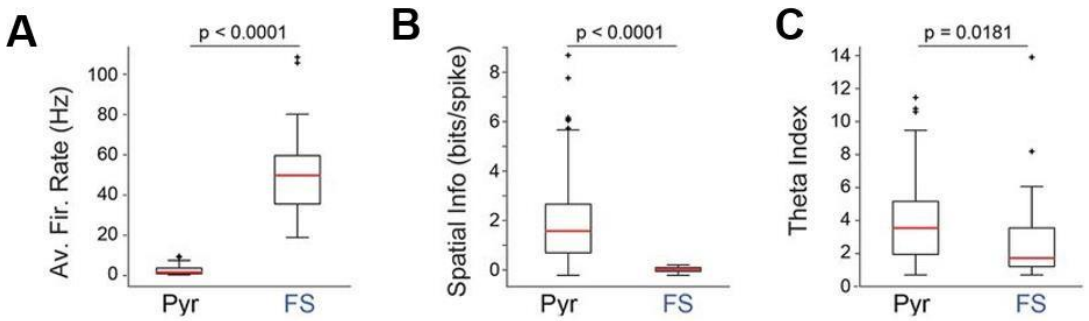

Figure 7 Comparison of average firing rate, spatial information and theta index of putative pyramidal neurons and fast-spiking interneurons.

(A) Boxplot showing average firing rates for pyramidal cells (Pyr, n = 140) and fast-spiking interneurons recordings (FS, n = 19). Whiskers indicate 1.5 interquartile ranges. Outliers are shown as crosses. P values are indicated (Wilcoxon rank-sum test). Same statistical analysis and data visualization for B,C.

(B) Boxplot showing spatial information per spike for Pyr and FS recordings (Pyr, n = 140; FS, n = 19).

(C) Boxplot showing theta index for Pyr and FS recordings (C: Pyr, n = 111; FS, n = 19).

Adapted from (Ding et al., 2020).

The CA2 subfield of the hippocampus is a narrow and less studied region compared to its CA1 and CA3 neighbours, but it has been receiving more attention because of its unique role in hippocampal information processing, especially in social memory (Hitti & Siegelbaum, 2014; Wintzer et al., 2014). The anatomical borders of the CA2 have been defined according to different molecular and anatomical criteria. In our study, we defined the anatomic border of CA2 region by using the immunochemical marker PCP4 (see in **Figure 8A,C**). PCP4 expression largely overlaps with other commonly used CA2 markers (Kohara et al., 2014; Lein et al., 2005). However, there are scattered PCP4 positive (PCP4+) cells outside the CA2 region, especially on the distal CA3 side. Indeed, consistent with this idea, the two recorded and labelled PCP4+ neurons in freely moving mice in the CA3a region (**Figure 8**). They displayed characteristics more similar to CA2 pyramidal neurons both electrophysiological and morphologically. They both tended to fire bursting spikes and had a high ratio of dendrites in the SLM (see also **Figure 11**); more importantly, they lacked the typical thorny excrescences which were found in all other CA3 cells we recorded (**Figure 8B,D**). Thus, we speculate that CA3a

PCP4+ neurons might represent displaced CA2 cells within the CA3 field.

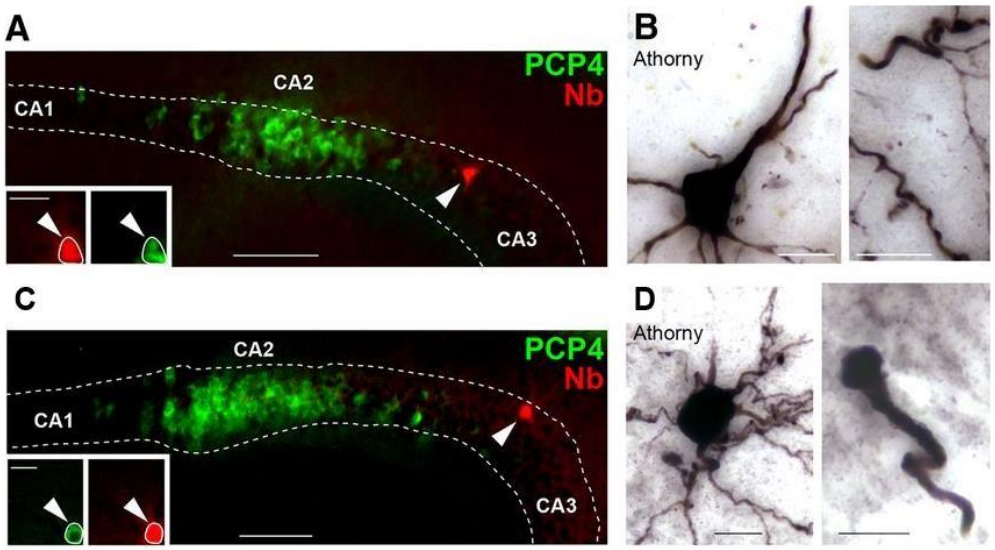

Figure 8 Identified PCP4+ CA3a pyramidal neurons.
(A) A PCP4+ CA3a pyramidal neuron recorded in freely-moving mice (red: neurobiotin, NB; Green: PCP4), recorded in freely-moving mice (indicated by 1 in **Figure 11**). Bottom left, High-magnification view of the cell soma. Scale bars: 100 μm; Inset, 20 μm.
(B) Proximal dendritic morphology for the neuron in A, shown by maximum intensity z-stack projection after DAB conversion. Note the smooth proximal dendrites without thorny excrescences. Scale bars, 15 μm.
(C–D) Same as in A–B, but for another PCP4-positive CA3a Pyr, recorded in freely-moving mice (indicated by 2 in **Figure 11**). Scale bars, same as in A–B.
Adapted from (Ding et al., 2020).

We next compared the spatial coding properties of CA2 and CA3 pyramidal neurons. For simplicity, we divided CA3 region into CA3a, CA3b, and CA3c subregions along the proximal-distal axis. As expected, we found that a considerable fraction of neurons in all subfields displayed classical place cell firing patterns (19 of 50 active neurons), i.e. with one place field in the recording arena. The CA3 region tended to have a higher portion of place cells (15 of 35 recorded CA3 pyramidal cells and 4 of 15 recorded CA2 pyramidal cells were classified as place cell), while the CA2 region place cells displayed smaller receptive fields and higher in-field firing rates (**Figure 9**).

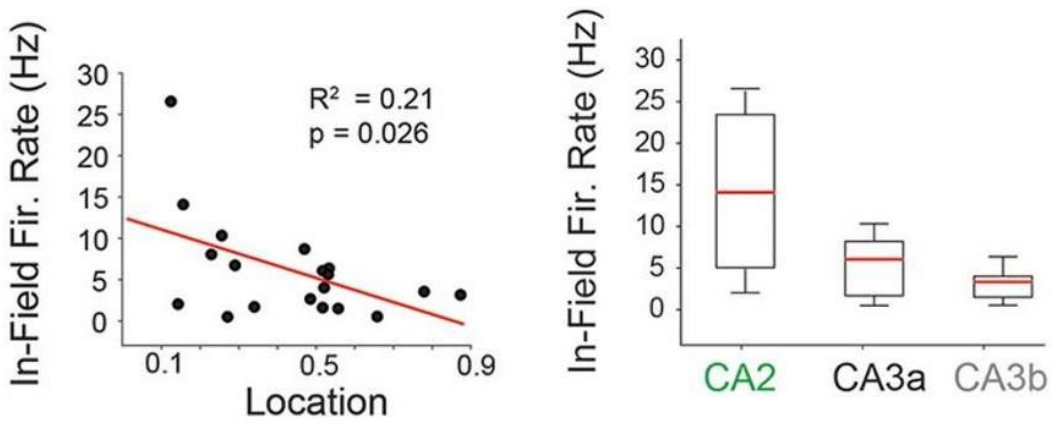

Figure 9 Average in-field firing rates of identified CA2 and CA3 place cells
Left, scatter plot showing the correlation of average in-field firing rate and cell proximodistal location for CA2/3 place cells (n = 19). 0 indicates the CA2/CA1 border; 1 indicates the most proximal end of CA3b. Red represents linear regression line. R^2 and p values are indicated.
Right, same data as in A, but grouped by subregions (CA2, n = 4; CA3a, n = 9; CA3b, n = 6). Whiskers indicate 1.5 interquartile range.
Adapted from (Ding et al., 2020).

We also analysed burst-firing properties of the neurons in relation to their anatomical location. The tendency of spiking in burst of a cell is computed as the burst index, defined as the fraction of spikes fired within bursts (spikes with inter-spike intervals lower than 6 ms). The proximal and distal position of a cell was calculated as its relative position along CA2 distal end (defined as position 0) to CA3b proximal end (defined as position 1). We found that the burst firing properties of the neuron were correlated to their topographical location along the proximal-distal axis, that is the more proximal the cell was located, the higher the tendency to fire spike bursts (**Figure 10A,B,C**). Burst propensity was organized along the CA2, CA3a and CA3b axis (**Figure 10D,E**), in line with previous work (Oliva et al., 2016). The pyramidal neurons in CA2 tended to spike in burst most frequently, followed by neurons in CA3a and CA3b region.

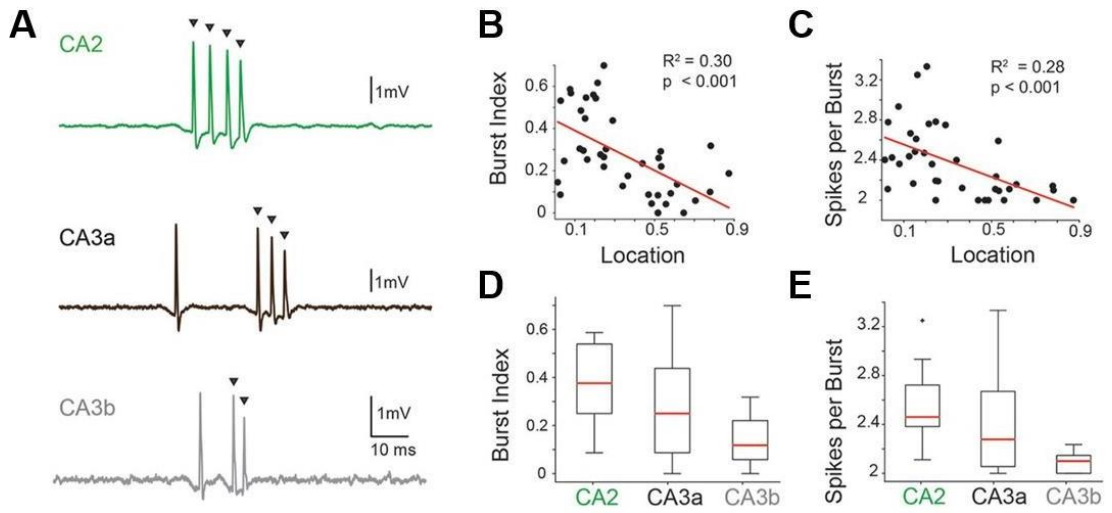

Figure 10 Burst firing properties of CA2 and CA3 pyramidal neurons recorded in freely-moving mice.

(A) Representative high-pass filtered spike traces of a CA2 (green), a CA3a (black), and a CA3b (gray). Black triangles represent spikes in burst (ISI ≤ 6 ms).

(B) Scatter plot showing the correlation of burst index and cell proximodistal location. 0 indicates the CA2/CA1 border; 1 indicates the most proximal end of CA3b. Red represents linear regression line. R^2 and p values are indicated. (n = 40).

(C) Same as in B, but for the average number of spikes per burst.

(D) Same data as in B, but grouped by subregions. Whiskers indicate 1.5 interquartile range.

(E) Same data as in C, but grouped by subregions. Whiskers indicate 1.5 interquartile range. Outliers are indicated as crosses.

Adapted from (Ding et al., 2020).

We further investigated in vivo spiking patterns in relation to neuronal dendritic morphology in CA2 and CA3 pyramidal cells. We reconstructed the dendritic tree of 17 pyramidal neurons from freely-moving recordings with high-quality dendritic fillings of Neurobiotin. Consistent with the literature (Ishizuka et al., 1995; Sun et al., 2017), we found that the cells located in more distal regions had a relatively larger amount of dendritic tree in SLM (**Figure 11**). More interestingly, we found a positive correlation between the apical dendritic ratio in SLM to the neuron's in vivo burst firing propensity, suggesting that the entorhinal input (selective for the SLM) might impose a bursty firing pattern on CA2/CA3 pyramidal neurons during natural behaviour (**Figure 11**).

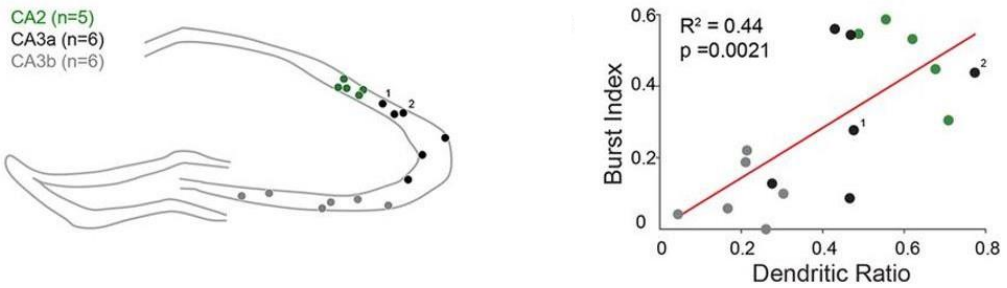

Figure 11 Morphologic correlates of spike-burst activity in CA2 and CA3 neurons.
Left, somatic location of the reconstructed pyramidal neurons along the proximal-distal axis of CA2/CA3 pyramidal layer included in the bustiness analysis: CA2 neurons (green, n = 5), CA3a neurons (black, n = 6), CA3b neurons (gray, n = 6). The two numbers (1, 2) indicate the two PCP4+ CA3a neurons (see also **Figure 8**).
(B) Scatter plot showing the correlation of burst index and dendritic ratio (see Materials and Methods and **Figure 4**) of the same cells shown in A. Red represents linear regression line. R^2 and p values are indicated.
Adapted from (Ding et al., 2020).

Together, our findings show that the relative amount of dendritic length in the SLM (sampling entorhinal inputs) corresponds with the burst tendency of individual pyramidal neurons along the CA2/CA3 proximodistal axis. We suggest that the relative weights of entorhinal and associational inputs control individual CA2 and CA3 neurons burst spiking activity during spatial exploration in vivo.

3.2 Structure-function relationships of CA1 pyramidal neurons.

3.2.1 Preferential recruitment of Calb1-negative CA1 pyramidal neurons in spatial representation

We first validated the efficiency and reliability of the opto-tagging method in the juxtacellular recording configuration. We first selectively expressed ChR2 in Calb1+ cells in the dorsal CA1 with the help of the Calb1^{cre} transgenic mouse line and AAV-flex-ChR2 virus (see details in Materials and Methods, **Figure 12**). Under anaesthesia, we recorded and labelled single cells in the CA1 region juxtacellularly. During the recordings, we stimulated the cell with 473nm laser light to test for light-evoked spike responses. We found cells that reliably responded to light stimuli, and those cells were confirmed to be positive for both Calb1 and ChR2 histochemically post hoc (n = 10, see one representative cell in **Figure 13** with mean light evoked spike latency = 2.1±0.12 ms). On the other hand, all identified neurons where light evoked spiked were not observed, were found to be negative for both Calb1 and ChR2 (n = 7). These data indicated that under our opto-juxtacellular configuration, evoked spike responses to light stimulation can inform about the cell identity (i.e. Calb1+ versus Calb1-).

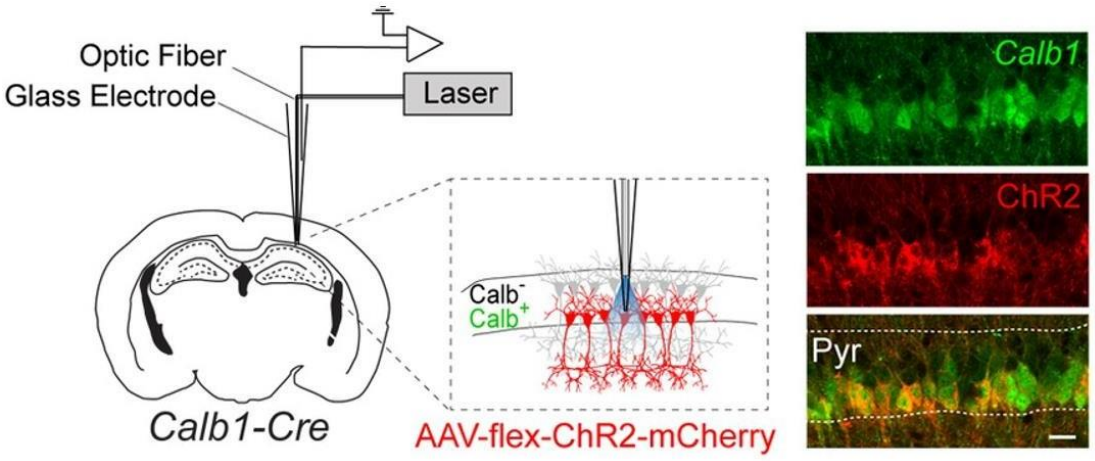

Figure 12 Juxtacellular opto-tagging configuration of CA1 Calb1+ pyramidal neurons
Left, schematic illustration of juxtacellular opto-tagging recording configuration. Viral vector (e.g., AAV-flex-ChR2-mCherry) is injected into the dorsal CA1 region of Calb1^{cre} mice, enabling selective expression of ChR2 in CA1 Calb1+ pyramidal neurons. Single neuron activities are recorded juxtacellularly by glass electrode with optic fiber inside in dorsal CA1. Right, a confocal image showing the colocalization of ChR2 (red, coexpressed with mCherry) and Calbindin (green) in superficial CA1 pyramidal neurons. Scale bar = 20 μm.
Adapted from (Ding et al., 2022).

Although the CA1 is known for its low recurrent connections (Vanderwolf, 1969), we sought to confirm that directly light-activated cells (ChR2+) can be distinguished from indirectly activated cells (ChR2- but activated by axonal input) based on the latency of the evoked spikes. We therefore performed axonal activation in both mossy fiber and Schaffer Collaterals synapses by expressing ChR2 in DG while recording in CA3 or expressing ChR2 in CA3 while recording CA1 cells (**Figure 14 and Figure 15**). We found that, although some neurons could be reliably activated by light stimulations of axonal inputs, those indirectly-activated cells had a significantly longer spiking latency.

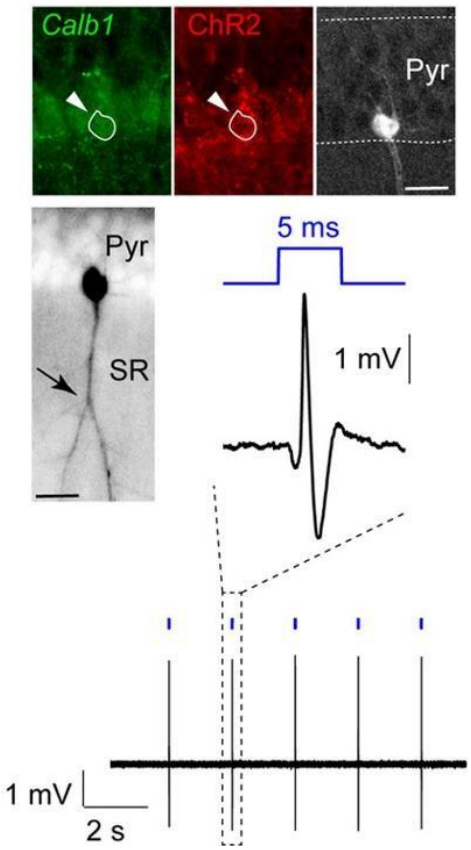

Figure 13 A representative light-responsive CA1 Calb1+ pyramidal neuron, recorded in vivo.
Top, epifluorescence images of a recorded light-responsive CA1 Calb1+ (green) and ChR2+ (red), labelled with Neurobiotin (white).
Middle, inverted signal z-stack projection of the same neuron. Branching point of the primary apical dendrite indicated by an arrowhead.
Bottom, juxtacellular spike trace (high-pass filtered) showing spike responses upon blue light pulses (blue, 5 ms). Scale bar = 20 µm.
Adapted from (Ding et al., 2022).

AAV-CAG-ChR2-mCherry was injected in the CA3 region of wild-type mice, expressing ChR2 in Schaffer collaterals terminals (**Figure 14**). Eleven light-activated pyramidal neurons were recorded in the CA1 region, which displayed a mean light evoked spike latency of 7.0 ± 1.8 ms. On the other hand, ChR2 (or oChIEF) were expressed in the DG granule cells and mossy fiber projections with the help of AAV-hSyn1-flex-ChR2-mCherry (or AAV-hSyn1-flex-oChIEF-TdTomato) and Calb1^{cre} mice (**Figure 15**). We then recorded in the CA3 region and identified a subset of light activated pyramidal neurons. Those neurons also displayed a longer mean latency of

8.1 ± 2.4 ms (n = 7). In both of synaptically light activated configurations, light activated neurons displayed significantly higher latencies compare to directly light activated CA1 pyramidal neurons (as in **Figure 12**, directly activated neurons mean latency = 2.7 ± 0.3 ms, n = 10; Kruskal–Wallis multiple group comparison p = 0.00006). Thus, based on our data and post-hoc histological validation, a threshold of 4 ms on light evoked spike latency was found to reliably separate directly from indirectly light-activated neurons. To this end, we benchmarked juxtacellular opto-tagging in hippocampal pyramidal neurons and showed the technical feasibility of this method.

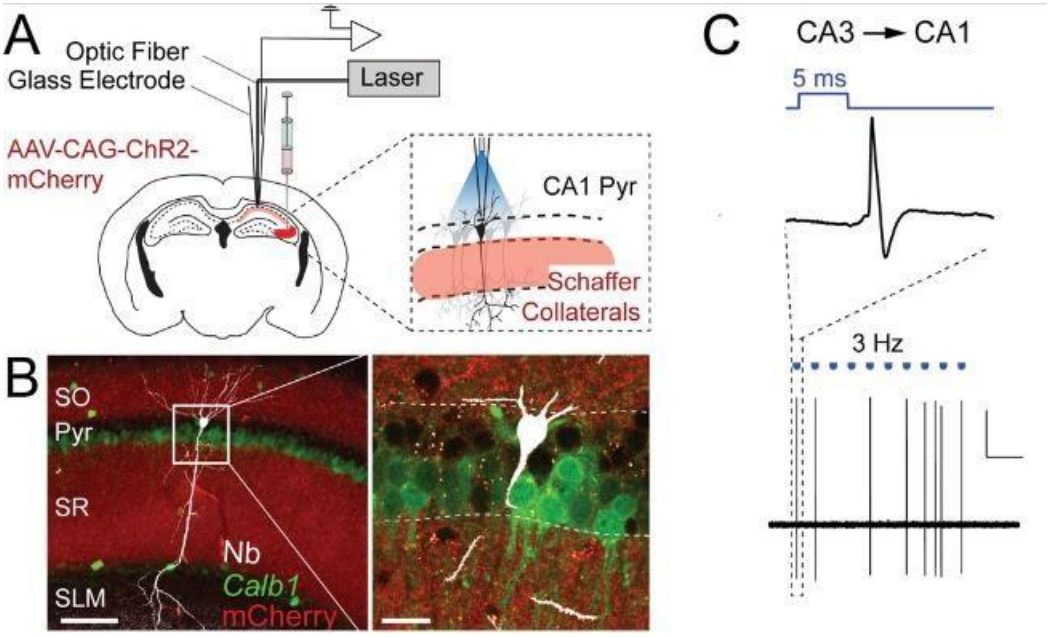

Figure 14 Juxtacellular opto-activation of Schaffer collaterals inputs onto CA1 neurons in anesthetized mice.

(A) Schematic illustration of juxtacellular opto-activation of Schaffer collaterals inputs onto CA1 neurons.

(B) Confocal images of a light-responsive CA1 pyramidal neuron (recording shown in C). High-magnification view on the right. The neuron (labelled with Neurobiotin, white) is positive for ChR2 (red, coexpressed with mCherry) but negative for Calb1 (green). Scale bars = 100 µm (left), 20 µm (right).

(C) High-pass filtered juxtacellular trace (bottom) for the neuron shown in B, showing unreliable and long latency spike responses upon blue light pulses (blue, 5 ms). Scale bar = 2 mV, 2 s.

Adapted from (Ding et al., 2022).

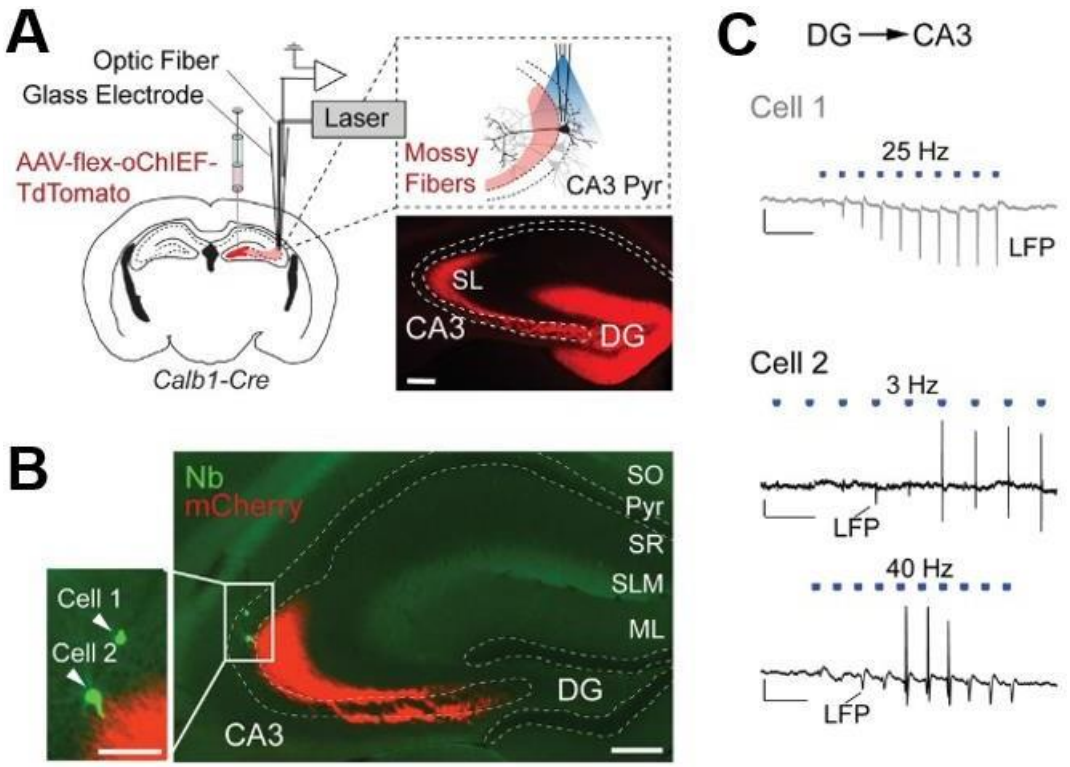

Figure 15 Juxtacellular opto-activation of mossy fiber inputs onto CA3 neurons in anesthetized mice.

(A) Schematic illustration of juxtacellular opto-activation of Schaffer collaterals mossy fiber inputs onto CA3 neurons. Viral vector (e.g., AAV-hSyn1-flex-oChIEF-TdTomato) was injected into the DG region of Calb1^{cre} mice. Right bottom, epifluorescence image showing DG injection site and mossy fiber projections (red, oChIEF-TdTomato) along the transverse CA3 axis.

(B) Epifluorescence images of a nonresponsive (Cell 1) and a responsive (Cell 2) CA3a pyramidal neuron recorded along the same electrode penetration (recordings shown in C). High-magnification view on the left. (green, Nb; red, oChIEF-TdTomato). Scale bars = 100 µm (left inset), 200 µm (right).

(C) Representative recordings of nonresponsive Cell 1 (top) and responsive Cell 2 (bottom) shown in B. Light activated spiking response was absent in Cell 1 (top, Scale bars = 2 mV, 100 ms), but Cell 2 showed unreliable spike responses upon blue light pulses (blue, 5 ms). Scale bars = 2 mV, 500 ms (middle trace); 2 mV, 50 ms (bottom trace).

Adapted from (Ding et al., 2022).

In the next step, we introduced opto-tagging procedures in the freely-moving recording configuration. In addition, we developed a novel mechanical micropositioning system that allowed micro-adjusting of the entry point of the electrode (**Figure 16**), thus enabling multiple attempts to be performed, higher mechanical stability and prolonged recording durations.

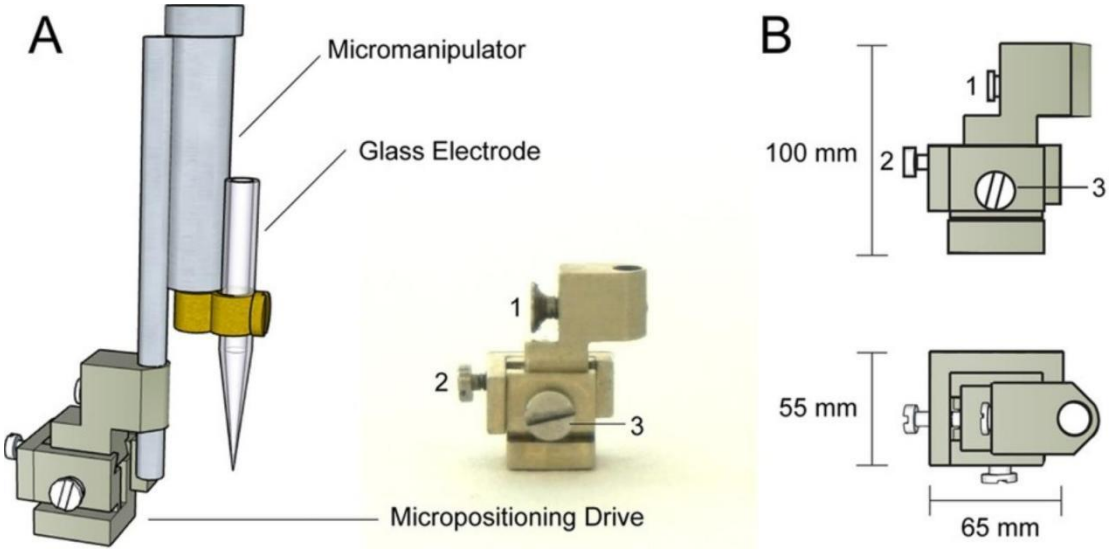

Figure 16 Micropositioning Drive enables lateral move of glass electrode penetrations.
(A) Left, 3D schematic representations of the Micropositioning Drive and micromanipulator assembly. Right, a side view picture of the Micropositioning Drive. Screw (1) secures the micromanipulator to the Micropositioning Drive; Screw (2) enables the later move of the micromanipulator; Screw (3) secures the Micropositioning Drive component that holds the micromanipulator.
(B) Side and top views of the Micropositioning drive (dimensions are shown).
Adapted from (Ding et al., 2022).

We recorded and opto-tagged CA1 neurons in mice exploring a circular arena (see also **Figure 3**). We found the typical activity of CA1 pyramidal neurons as a low firing rate (average firing rate, 2.16 ± 2.06 Hz; n = 54) and a tendency to fire complex spikes (average burst index, 0.28 ± 0.18, n = 45). Among the recorded cells, we found cells that responded to light stimulations robustly and with short latency (< 4 ms, as in **Figure 17**). Those cells were thus classified as Calb1+ neurons.

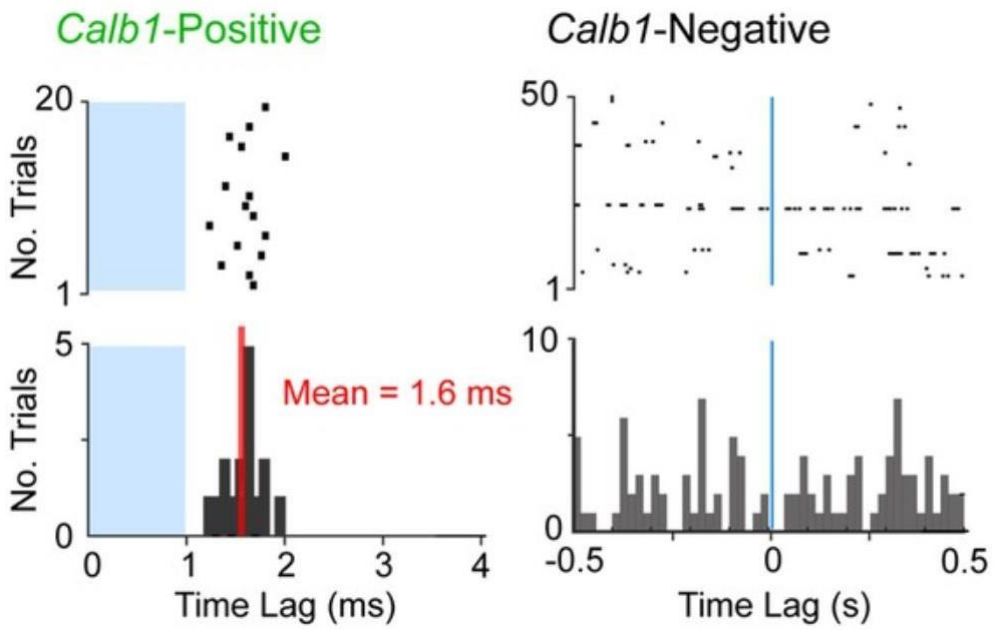

Figure 17 Representative opto-tagging responses of Calb1+ and Calb1- cells from freely-moving recordings.

Left, raster plots (top) and peristimulus time histograms (bottom) showing responses from a Calb1+ neuron to the light stimulus (blue, 1 ms pulses, 20 trails), recorded in a freely-moving mouse (mean spiking latency indicated).

Right, same as left panel but for a Calb1- neuron with larger time window and bin size. Note the absence of response to light pulses in the Calb1- cell.

Adapted from (Ding et al., 2022).

Altogether, we recorded 15 CA1 Calb1+ and 39 Calb1- cells in freely moving mice (**Figure 18**, classified by opto-tagging or juxtacellular labelling). These two cell classes showed similar average firing rates (Calb1+ 2.17 ± 2.02 Hz, n = 15; Calb1- 2.15 ± 2.10 Hz, n = 39; p = 0.86) and burst index (Calb1+ 0.29 ± 0.21, n = 13; Calb1- 0.29 ± 0.18, n = 32; p = 0.97). However, Calb1-negative cells carried more spatial information, while Calb1+ cells showed a more diffuse spatial firing pattern (**Figure 19**, Spatial information per spike: Calb1+ 0.65 ± 0.35 bits/spike, n = 12; Calb1- 1.56 ± 0.79 bits/spike, n = 26; p = 0.0003; sparsity index Calb1+ 0.53 ± 0.15, n = 12; Calb1- 0.31 ± 0.17, n = 26; p = 0.0003), in line with previous observations from deep/superficial CA1 recordings (Geiller et al., 2017; Masurkar et al., 2020).

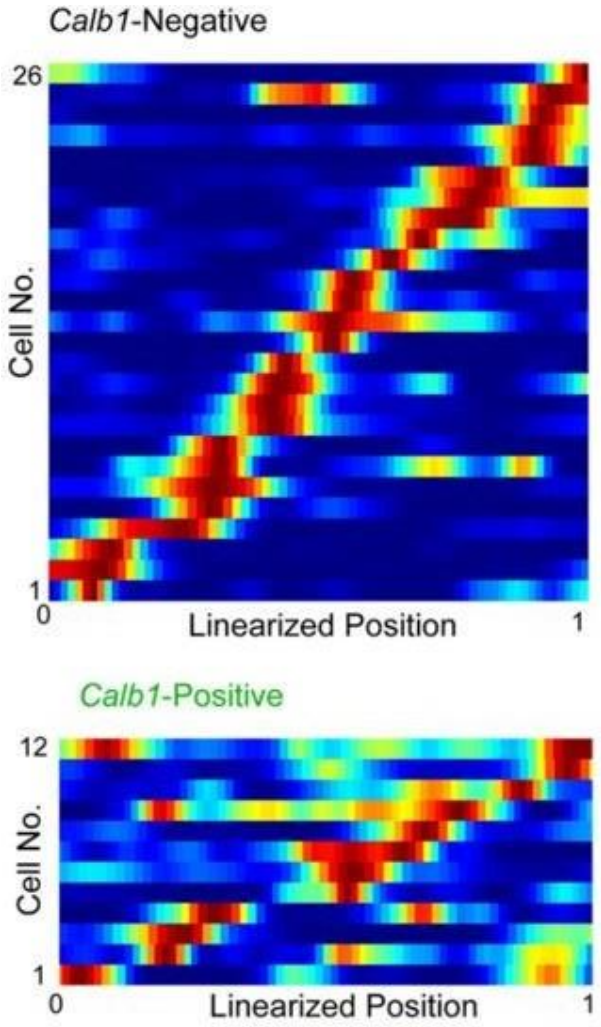

Figure 18 Spatial firing patterns of putative Calb1- and Calb1+ CA1 pyramidal neurons.
Top, linearized rate maps of all Calb1- cells (n = 26), showing in linearized 1D projection of the recording arena (see in Materials and Methods). Cells are ordered by maximal firing position in the linearized trajectory.
Bottom, same as in top except for Calb1+ cells (n = 12).
Adapted from (Ding et al., 2022).

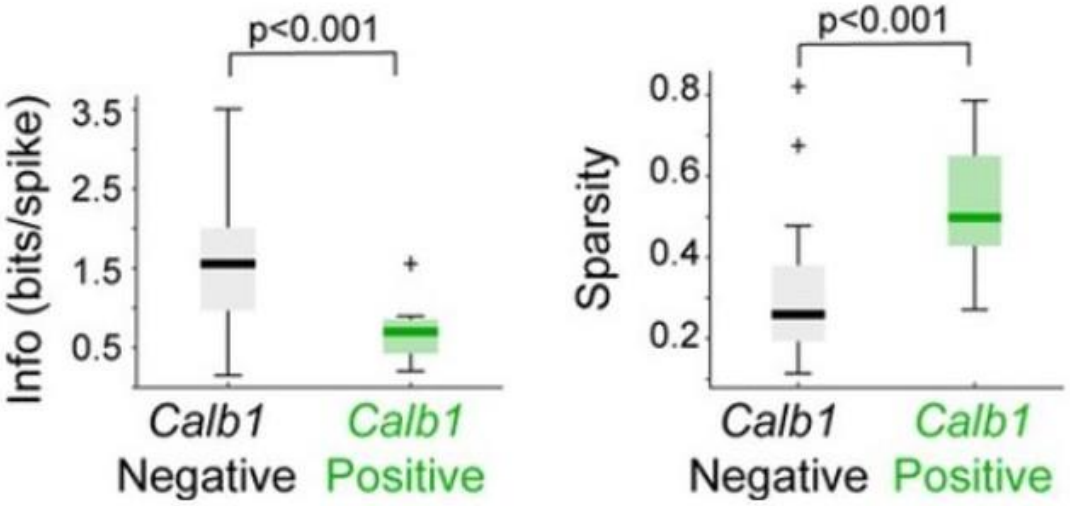

Figure 19 Statistical comparison of spatial-temporal properties of Calb1+ and Calb1- neurons recorded in freely-moving animals

Left, spatial information comparison of Calb1- (n = 26, same as in **Figure 18** top panel) and Calb1+ (n = 12, same as in **Figure 18** bottom panel) CA1 neurons. p value is indicated (Wilcoxon rank-sum test). Black/green lines indicate medians. Outliers are shown as crosses.

Right, same as in the left but for the comparison of sparsity.

Adapted from (Ding et al., 2022).

Furthermore, we provided evidence that our methods can also be used for recording, opto-tagging and labelling interneurons in in anesthetized (**Figure 20**) and freely-moving mice (**Figure 21**). These proof-of-principle data indicate that our technique can also be used for resolving structure-function relationships of sparser cell types, e.g., interneurons.

In summary, we performed ChR2-assisted juxtacellular recordings in freely moving mice. We believe this method will complement other neuroscience recording techniques to promote structure-function analysis of neuronal circuits during natural behaviours.

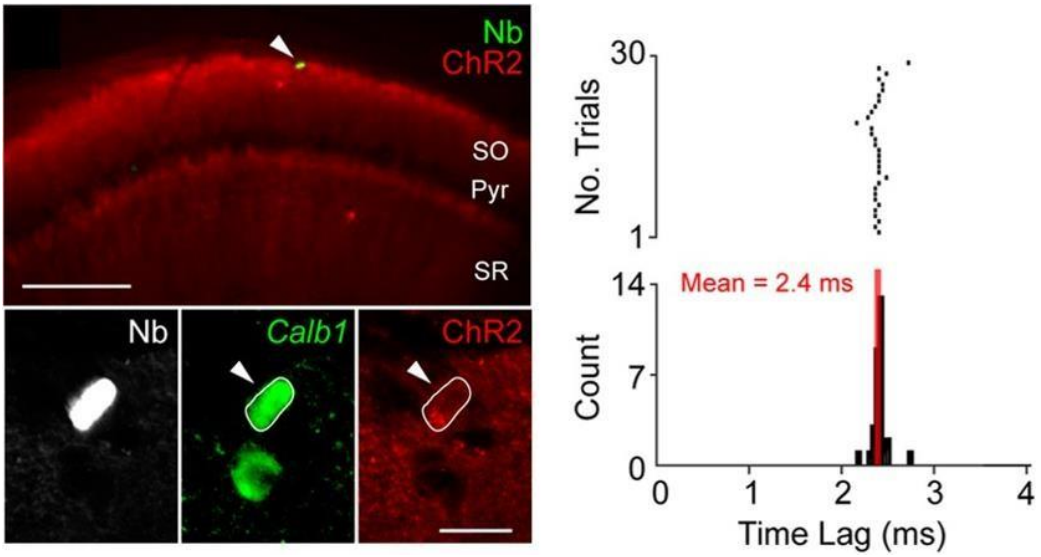

Figure 20 A juxtacellularly opto-tagged of Calb1+ interneuron in anaesthesia.
Left, epifluorescence images showing a juxtacellularly recorded, opto-tagged and identified Calb1+ interneuron in vivo (Neurobiotin, white; Calb1, green; ChR2, red). Scale bar = 200 μm (top) and 20 μm (bottom).
Right, raster plot (top) and peristimulus time histogram (bottom) showing the spike responses to the light stimulus (5ms, 30 trails) for the same interneuron. The average latency is indicated. Adapted from (Ding et al., 2022).

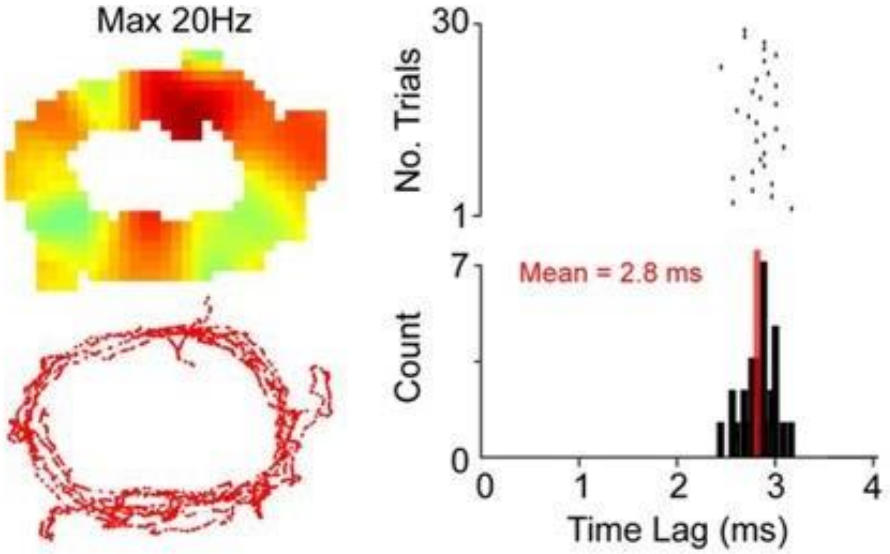

Figure 21 Representative juxtacellular opto-tagging of Calb1+ interneurons in freely-moving mice.
Left, color-coded rate map (top) and spike-trajectory plot (bottom) of a putative Calb1+ interneuron recorded in a freely-moving mouse.
Right, raster plot (top) and peristimulus time histogram (bottom) showing the spike responses to the light stimulus (1ms, 30 trails) for the same interneuron. The average latency is indicated. Adapted from (Ding et al., 2022).

3.2.2 Preferential recruitment of AcD CA1 pyramidal neurons in ripple activity

The juxtacellular technique can provide unique data which is hard to access with alternative electrophysiology methods. For example, juxtacellular labelling offers the means to explore structural neuronal features that are not accessible with alternative electrophysiology techniques, e.g. extracellular recordings.

We recorded CA1 neurons in awake head-fixed mice; in addition, a silicon probe was placed in close proximity to record LFP (Hodapp et al., 2022). In awake animals, we observed strong and reliable ripple activities both in the juxtacellular and in the silicon probe signals. The recorded cells were further filled with Neurobiotin and their morphology was reconstructed ex vivo. About 50% of the identified cells were found to have an axon that originated from a basal dendrite. Thus, CA1 neurons were classified into two categories: the ones with an axon-carrying dendrite (AcD cells) or the ones without (nonAcD cells). During in vivo recording, compared to nonAcD cells, AcD neurons displayed a ~4.5-fold higher probability to fire during ripples, and the firing frequency during ripples was ~2.5 fold higher. No difference in firing rate outside ripples was found between these two types of cells. These results indicate that mechanism may exist in AcD cells that enables them to escape the global inhibition during events like ripples, allowing them to spike and to be preferentially recruited.

Further studies were carried out in brain slices and computer modeling to explore how the structural differences between AcD and nonAcD cells could contribute to their different recruitment probabilities during ripples (Hodapp et al., 2022). A general hypothesis was proposed that the excitatory input onto those axon-carrying dendrites can escape the perisomatic inhibitory input, thus increasing the propensity of firing in events like ripples.

4. DISCUSSION AND CONCLUSION

Resolving structure-function relationships is a fundamental step in understanding the mechanics of brain functions. Great success has been achieved in obtaining the electrophysiology features of large amount of neurons and deciphering their functions *in vivo*. A vast effort has been invested in brain slice studies to understand single cell-intrinsic properties, connectivity, and microcircuit. However, linking those features to single neuron morphology from an intact system has been elusive. In my work, I took advantage of juxtacellular recording in vivo for filling this gap.

With relatively low constraints of mechanical stability and a relatively high success rate compared to e.g. the whole-cell configuration, juxtacellular recordings in freely moving mice can be currently seen as the method of choice for resolving structure-function relationship of the CA2/CA3 neurons (**Figure 6**). We recorded and labelled CA2 and CA3 pyramidal neurons in freely-moving mice and found that the in vivo activity pattern of single neurons highly correlated with their topographical location (namely the location along the transverse axis). Place cells were recorded in both CA2 and CA3 regions, with a slightly lower potion in CA2 region. However, the CA2 place cells tended to have sharper place fields and higher in-field firing rates. Even though on average, CA2 cells were less spatially modulated than CA3 cells. Together with evidence from extracellular recordings, CA2 pyramidal cells carried less spatial information and tended to remap rapidly, indicating a non-spatial coding functionality of this region. Further work needs to be carried out to resolve the structure-function relationship within the CA2 region itself, since functional diversity (Fernandez-Lamo et al., 2019; Kohara et al., 2014) and morphology heterogeneity (Bartesaghi & Ravasi, 1999; Helton et al., 2019) were both reported in this region.

Moreover, our results showed that the burst spiking tendency of single cells strongly correlated to their dendritic ratio in SLM, where the entorhinal input reaches CA2/CA3 (**Figure 11**). Together with evidence from brain slice studies, the strength of entorhinal input decreased from distal to proximal end as well as dendritic length in SLM of

CA2/CA3 pyramidal cells (Ishizuka et al., 1995; Sun et al., 2017). We thus hypothesized that the input from the entorhinal cortex could determine the temporal spiking properties of CA2/CA3 pyramidal cells during natural behaviour.

Burst spiking has been described in a range of neuron types (Krahe & Gabbiani, 2004; Lisman, 1997) and is thought to be essential in neural circuit computation. Burst spiking of neurons is proposed to be important in both forming and retrieving memory (Kaifosh & Losonczy, 2016; Treves & Rolls, 1992). During memory formation, the CA3 region is thought to perform pattern completion. Episodic information from the entorhinal cortex first activates a subset of neurons in CA3 and CA2. Via the strong recurrent circuit of CA3, activation of neuron assembly is further completed, and the memory engram is retrieved. A recent study has shown that all CA3 pyramidal neurons can generate burst action potentials (Raus Balind et al., 2019). However, from our result, when the animal was exploring a familiar environment, burst activity was preferentially contributed by those cells with longer dendritic segments in SLM. Thus, we propose that these cells might act as “drivers” in pattern completion process of memory retrieving.

Our results proved that juxtacellular recording is a powerful method for resolving single-cell structure-function relationships. However, a significant limitation of this method is that the sampling procedure is "blind" to the experimenter. Targeting a pre-defined cell class can be extremely challenging, depending on its relative abundance in the brain region of interest. To circumvent this limitation, we combined opto-tagging and juxtacellular recording procedures.

The opto-tagging technique is readily combined with extracellular recording methods in freely behaving animals (Anikeeva et al., 2011; Beyeler et al., 2016; Roux et al., 2014). Extracellular opto-tagging is achieved by restricting the expression of ChR2 (or other opsins) in pre-defined cell populations. During the natural behaviour of the animals, photostimulated cell activation (or inhibition) in those cells can be recorded extracellularly, thus linking in vivo activity to cell type. However, the identification of cells is indirect in this method because it purely relies on neuronal spiking responses to

light stimuli. During periods of highly synchronous activity, as occurring for example during light stimulation, the detection of spikes is known to be particularly unreliable (Roux et al., 2014; Stark et al., 2012). Moreover, separating directly and indirectly light-activated neurons remains challenging, since spike response latency can be similarly short in a high recurrent circuit, and no post hoc cell identification can be accessed by extracellular recording methods. Combining opto-tagging and juxtacellular recording techniques can circumvent these limitations.

The high signal-to-noise ratio of juxtacellular recordings provides unequivocal spike identification. The morphological identification of the recorded cell can be further examined post hoc, thus providing the "ground truth" of directly or indirectly activation of the light stimulation of the labelled cell. In the CA1 region, we found that a threshold of 4ms could reliably separate directly from indirectly light activated pyramidal neurons. Although variability exists with different light power and expression levels, all identified ChR2+ neurons had evoked spiking latency lower than 4ms while syntactically activated ChR2- neurons had higher than 4ms.

To test the combination of opto-tagging and juxtacellular recording techniques, we chose the CA1 region as our test ground. CA1 superficial neurons are particularly difficult to record with conventional (‘blind’) juxtacellular recording techniques because of their anatomical location. The Calb1^{cre} transgenic mouse line enabled restricted expression of ChR2 in CA1 superficial neurons. Combining opto-tagging and juxtacellular recording techniques successfully increased the sampling rate of CA1 Calb+ superficial cells in freely moving mice, thus offering a proof-of-principle validation of this technique (**Figure 18**).

Our result showed that the Calb1+ superficial neurons were weakly spatially modulated while most 'place cells' were recruited from the Calb1- deep pyramidal neurons in CA1, in line with previous studies (Danielson et al., 2016; Fattahi et al., 2018; Geiller et al., 2017; Henriksen et al., 2010; Mizuseki et al., 2011). Our data confirmed functional heterogeneity among deep and superficial CA1 cells. Recent studies showed that LEC projects preferentially to superficial CA1 cells, thus weaker

spatial modulation of the Calb1+ neurons may be caused by upstream information input. Further studies need to be carried out to explore the function of the Calb1+ in vivo.

The opto-tagging juxtacellular recording technique is a valid complement to existing in-vivo recording and cell-identification techniques with higher structural and functional resolution. We presented an application of the technique related to the targeting of a 'ubiquitous' cell population (Calb1- CA1 superficial pyramidal cells). In principle, the method can also be applied to sparser neuronal populations – like specific subtypes of interneurons – which are difficult to sample via 'blind' search procedures. We also provided proof-of-principle evidence that Calb1-positive interneurons can also be recorded with our technique

With the juxtacellular technique, we further investigated the contribution of distinct CA1 pyramidal cell types to hippocampal ripples. In vivo juxtacellular recording and labelling showed similar results as in acute brain slices: the differential participation of CA1 cells to ripples as a function of their axon initial segment (AIS) placement (Hodapp et al., 2022). Neurons with an "Axon carry Dendrite" (AcD cell) had a significantly higher chance to spike during ripples. Additional computational modelling and in vitro slice physiology showed that the excitatory input to axon-carrying dendrite is capable of escaping the preromantic inhibition, thus enabling the participation of AcD cells (but not of non-AcD cells) to ripple events (Hodapp et al., 2022).

In summary, single-cell recordings of hippocampal neurons in naturally behaving mice allowed us to explore several dimensions of functional and structural neuronal heterogeneity. My work provided evidence for relationships between morphological / chemohistological neuronal identity and in-vivo activity. In CA2 and CA3 regions, neuron burst spiking behaviour correlated to dendrite ratios in SLM. In the CA1 region, neuronal spatial modulation correlated to its radial location and Calb1 expression, and neuron spiking activity during ripples related to the axon initial segment placement. Methodologically, we performed juxtacellular recording and labelling technique in anesthetized, awake head-fixed, and freely moving mice, and further combined it with

the optogenetic technique to improve sampling of a predefined cell population. Taken together the findings and methodology advances improved our understanding of structure-function relationships in mouse hippocampus and would promote further studies in resolving hippocampal memory computation.

5. REFERENCES

Andersen, P. (1960). Interhippocampal impulses. II. Apical dendritic activation of CAI neurons. *Acta Physiol Scand*, *48*, 178-208. https://doi.org/10.1111/j.1748-1716.1960.tb01858.x

Andersen, P., Eccles, J. C., & Loyning, Y. (1964). Location of Postsynaptic Inhibitory Synapses on Hippocampal Pyramids. *J Neurophysiol*, *27*, 592-607. https://doi.org/10.1152/jn.1964.27.4.592

Anderson, M. I., & Jeffery, K. J. (2003). Heterogeneous modulation of place cell firing by changes in context. *J Neurosci*, *23*(26), 8827-8835. https://www.ncbi.nlm.nih.gov/pubmed/14523083

Anikeeva, P., Andalman, A. S., Witten, I., Warden, M., Goshen, I., Grosenick, L., Gunaydin, L. A., Frank, L. M., & Deisseroth, K. (2011). Optetrode: a multichannel readout for optogenetic control in freely moving mice. *Nat Neurosci*, *15*(1), 163-170. https://doi.org/10.1038/nn.2992

Bartesaghi, R., & Ravasi, L. (1999). Pyramidal neuron types in field CA2 of the guinea pig. *Brain Res Bull*, *50*(4), 263-273. https://doi.org/10.1016/s0361-9230(99)00198-7

Beyeler, A., Namburi, P., Glober, G. F., Simonnet, C., Calhoon, G. G., Conyers, G. F., Luck, R., Wildes, C. P., & Tye, K. M. (2016). Divergent Routing of Positive and Negative Information from the Amygdala during Memory Retrieval. *Neuron*, *90*(2), 348-361. https://doi.org/10.1016/j.neuron.2016.03.004

Botcher, N. A., Falck, J. E., Thomson, A. M., & Mercer, A. (2014). Distribution of interneurons in the CA2 region of the rat hippocampus. *Front Neuroanat*, *8*, 104. https://doi.org/10.3389/fnana.2014.00104

Burgalossi, A., Herfst, L., von Heimendahl, M., Forste, H., Haskic, K., Schmidt, M., & Brecht, M. (2011). Microcircuits of functionally identified neurons in the rat medial entorhinal cortex. *Neuron*, *70*(4), 773-786. https://doi.org/10.1016/j.neuron.2011.04.003

Correll, R. E., & Scoville, W. B. (1967). Significance of delay in the performance of monkeys with medial temporal lobe resections. *Exp Brain Res*, *4*(1), 85-96. https://doi.org/10.1007/BF00235220

Cragg, B. G., & Hamlyn, L. H. (1955). Action potentials of the pyramidal neurones in the hippocampus of the rabbit. *J Physiol*, *129*(3), 608-627. https://doi.org/10.1113/jphysiol.1955.sp005382

Csicsvari, J., Hirase, H., Czurko, A., Mamiya, A., & Buzsaki, G. (1999). Oscillatory coupling of hippocampal pyramidal cells and interneurons in the behaving Rat. *J Neurosci*, *19*(1), 274-287. https://www.ncbi.nlm.nih.gov/pubmed/9870957

Daigle, T. L., Madisen, L., Hage, T. A., Valley, M. T., Knoblich, U., Larsen, R. S., Takeno, M. M., Huang, L., Gu, H., Larsen, R., Mills, M., Bosma-Moody, A., Siverts, L. A., Walker, M., Graybuck, L. T., Yao, Z., Fong, O., Nguyen, T. N., Garren, E., . . . Zeng, H. (2018). A Suite of Transgenic Driver and Reporter Mouse Lines with Enhanced Brain-Cell-Type Targeting and Functionality. *Cell*, *174*(2), 465-480 e422. https://doi.org/10.1016/j.cell.2018.06.035

Danielson, N. B., Zaremba, J. D., Kaifosh, P., Bowler, J., Ladow, M., & Losonczy, A. (2016). Sublayer-Specific Coding Dynamics during Spatial Navigation and Learning in Hippocampal Area CA1. *Neuron*, *91*(3), 652-665. https://doi.org/10.1016/j.neuron.2016.06.020

Diamantaki, M., Coletta, S., Nasr, K., Zeraati, R., Laturnus, S., Berens, P., Preston-Ferrer, P., & Burgalossi, A. (2018). Manipulating Hippocampal Place Cell Activity by Single-Cell Stimulation in Freely Moving Mice. *Cell Rep*, *23*(1), 32-38. https://doi.org/10.1016/j.celrep.2018.03.031

Diamantaki, M., Frey, M., Berens, P., Preston-Ferrer, P., & Burgalossi, A. (2016). Sparse activity of identified dentate granule cells during spatial exploration. *Elife*, *5*. https://doi.org/10.7554/eLife.20252

Diamantaki, M., Frey, M., Preston-Ferrer, P., & Burgalossi, A. (2016). Priming Spatial Activity by Single-Cell Stimulation in the Dentate Gyrus of Freely Moving Rats. *Curr Biol*, *26*(4), 536-541. https://doi.org/10.1016/j.cub.2015.12.053

Ding, L., Balsamo, G., Chen, H., Blanco-Hernandez, E., Zouridis, I. S., Naumann, R., Preston-Ferrer, P., & Burgalossi, A. (2022). Juxtacellular opto-tagging of hippocampal CA1 neurons in freely moving mice. *Elife*, *11*. https://doi.org/10.7554/eLife.71720

Ding, L., Chen, H., Diamantaki, M., Coletta, S., Preston-Ferrer, P., & Burgalossi, A. (2020). Structural Correlates of CA2 and CA3 Pyramidal Cell Activity in Freely-Moving Mice. *J Neurosci*, *40*(30), 5797-5806. https://doi.org/10.1523/JNEUROSCI.0099-20.2020

Douglas, R. J., & Isaacson, R. L. (1964). Hippocampal lesions and activity. *Psychonomic Science*, *1*(1), 187-188.

Dudek, S. M., Alexander, G. M., & Farris, S. (2016). Rediscovering area CA2: unique properties and functions. *Nat Rev Neurosci*, *17*(2), 89-102. https://doi.org/10.1038/nrn.2015.22

Epsztein, J., Brecht, M., & Lee, A. K. (2011). Intracellular determinants of hippocampal CA1 place and silent cell activity in a novel environment. *Neuron*, *70*(1), 109-120. https://doi.org/10.1016/j.neuron.2011.03.006

Fattahi, M., Sharif, F., Geiller, T., & Royer, S. (2018). Differential Representation of Landmark and Self-Motion Information along the CA1 Radial Axis: Self-Motion Generated Place Fields Shift toward Landmarks during Septal Inactivation. *J Neurosci*, *38*(30), 6766-6778. https://doi.org/10.1523/JNEUROSCI.3211-17.2018

Fernandez-Lamo, I., Gomez-Dominguez, D., Sanchez-Aguilera, A., Oliva, A., Morales, A. V., Valero, M., Cid, E., Berenyi, A., & Menendez de la Prida, L. (2019). Proximodistal Organization of the CA2 Hippocampal Area. *Cell Rep*, *26*(7), 1734-1746 e1736. https://doi.org/10.1016/j.celrep.2019.01.060

Fox, S. E., & Ranck, J. B., Jr. (1981). Electrophysiological characteristics of hippocampal complex-spike cells and theta cells. *Exp Brain Res*, *41*(3-4), 399-410. https://doi.org/10.1007/BF00238898

Frank, L. M., Brown, E. N., & Wilson, M. (2000). Trajectory encoding in the hippocampus and entorhinal cortex. *Neuron*, *27*(1), 169-178. https://doi.org/10.1016/s0896-6273(00)00018-0

Fujita, Y., & Sakata, H. (1962). Electrophysiological properties of CA1 and CA2 apical dendrites of rabbit hippocampus. *J Neurophysiol*, *25*, 209-222. https://doi.org/10.1152/jn.1962.25.2.209

Fyhn, M., Hafting, T., Treves, A., Moser, M. B., & Moser, E. I. (2007). Hippocampal remapping and grid realignment in entorhinal cortex. *Nature*, *446*(7132), 190-194. https://doi.org/10.1038/nature05601

Geiller, T., Fattahi, M., Choi, J. S., & Royer, S. (2017). Place cells are more strongly tied to landmarks in deep than in superficial CA1. *Nat Commun*, *8*, 14531. https://doi.org/10.1038/ncomms14531

Gray, C. M., Maldonado, P. E., Wilson, M., & McNaughton, B. (1995). Tetrodes markedly improve the reliability and yield of multiple single-unit isolation from multi-unit recordings in cat striate cortex. *J Neurosci Methods*, *63*(1-2), 43-54. https://doi.org/10.1016/0165-0270(95)00085-2

Hayman, R. M., Chakraborty, S., Anderson, M. I., & Jeffery, K. J. (2003). Context-specific acquisition of location discrimination by hippocampal place cells. *Eur J Neurosci*, *18*(10), 2825-2834. https://doi.org/10.1111/j.1460-9568.2003.03035.x

Helton, T. D., Zhao, M., Farris, S., & Dudek, S. M. (2019). Diversity of dendritic

morphology and entorhinal cortex synaptic effectiveness in mouse CA2 pyramidal neurons. *Hippocampus*, *29*(2), 78-92. https://doi.org/10.1002/hipo.23012

Henriksen, E. J., Colgin, L. L., Barnes, C. A., Witter, M. P., Moser, M. B., & Moser, E. I. (2010). Spatial representation along the proximodistal axis of CA1. *Neuron*, *68*(1), 127-137. https://doi.org/10.1016/j.neuron.2010.08.042

Henze, D. A., Borhegyi, Z., Csicsvari, J., Mamiya, A., Harris, K. D., & Buzsaki, G. (2000). Intracellular features predicted by extracellular recordings in the hippocampus in vivo. *J Neurophysiol*, *84*(1), 390-400. https://doi.org/10.1152/jn.2000.84.1.390

Herfst, L., Burgalossi, A., Haskic, K., Tukker, J. J., Schmidt, M., & Brecht, M. (2012). Friction-based stabilization of juxtacellular recordings in freely moving rats. *J Neurophysiol*, *108*(2), 697-707. https://doi.org/10.1152/jn.00910.2011

Hitti, F. L., & Siegelbaum, S. A. (2014). The hippocampal CA2 region is essential for social memory. *Nature*, *508*(7494), 88-92. https://doi.org/10.1038/nature13028

Hodapp, A., Kaiser, M. E., Thome, C., Ding, L., Rozov, A., Klumpp, M., Stevens, N., Stingl, M., Sackmann, T., Lehmann, N., Draguhn, A., Burgalossi, A., Engelhardt, M., & Both, M. (2022). Dendritic axon origin enables information gating by perisomatic inhibition in pyramidal neurons. *Science*, *377*(6613), 1448-1452. https://doi.org/10.1126/science.abj1861

Holmgren, C., Harkany, T., Svennenfors, B., & Zilberter, Y. (2003). Pyramidal cell communication within local networks in layer 2/3 of rat neocortex. *J Physiol*, *551*(Pt 1), 139-153. https://doi.org/10.1113/jphysiol.2003.044784

Hunsaker, M. R., Rosenberg, J. S., & Kesner, R. P. (2008). The role of the dentate gyrus, CA3a,b, and CA3c for detecting spatial and environmental novelty. *Hippocampus*, *18*(10), 1064-1073. https://doi.org/10.1002/hipo.20464

Hunt, D. L., Linaro, D., Si, B., Romani, S., & Spruston, N. (2018). A novel pyramidal cell type promotes sharp-wave synchronization in the hippocampus. *Nat Neurosci*, *21*(7), 985-995. https://doi.org/10.1038/s41593-018-0172-7

Ishizuka, N., Cowan, W. M., & Amaral, D. G. (1995). A quantitative analysis of the dendritic organization of pyramidal cells in the rat hippocampus. *J Comp Neurol*, *362*(1), 17-45. https://doi.org/10.1002/cne.903620103

Kaada, B. R., Rasmussen, E. W., & Kveim, O. (1961). Effects of hippocampal lesions on maze learning and retention in rats. *Exp Neurol*, *3*, 333-355. https://doi.org/10.1016/0014-4886(61)90009-7

Kaifosh, P., & Losonczy, A. (2016). Mnemonic Functions for Nonlinear Dendritic Integration in Hippocampal Pyramidal Circuits. *Neuron, 90*(3), 622-634. https://doi.org/10.1016/j.neuron.2016.03.019

Kandel, E. R., Spencer, W. A., & Brinley, F. J., Jr. (1961). Electrophysiology of hippocampal neurons. I. Sequential invasion and synaptic organization. *J Neurophysiol, 24*, 225-242. https://doi.org/10.1152/jn.1961.24.3.225

Kimble, D. P. (1963). The effects of bilateral hippocampal lesions in rats. *J Comp Physiol Psychol, 56*, 273-283. https://doi.org/10.1037/h0048903

Klausberger, T., Magill, P. J., Marton, L. F., Roberts, J. D., Cobden, P. M., Buzsaki, G., & Somogyi, P. (2003). Brain-state- and cell-type-specific firing of hippocampal interneurons in vivo. *Nature, 421*(6925), 844-848. https://doi.org/10.1038/nature01374

Kohara, K., Pignatelli, M., Rivest, A. J., Jung, H. Y., Kitamura, T., Suh, J., Frank, D., Kajikawa, K., Mise, N., Obata, Y., Wickersham, I. R., & Tonegawa, S. (2014). Cell type-specific genetic and optogenetic tools reveal hippocampal CA2 circuits. *Nat Neurosci, 17*(2), 269-279. https://doi.org/10.1038/nn.3614

Krahe, R., & Gabbiani, F. (2004). Burst firing in sensory systems. *Nat Rev Neurosci, 5*(1), 13-23. https://doi.org/10.1038/nrn1296

Kramis, R., Vanderwolf, C. H., & Bland, B. H. (1975). Two types of hippocampal rhythmical slow activity in both the rabbit and the rat: relations to behavior and effects of atropine, diethyl ether, urethane, and pentobarbital. *Exp Neurol, 49*(1 Pt 1), 58-85. https://doi.org/10.1016/0014-4886(75)90195-8

Lee, D., Lin, B. J., & Lee, A. K. (2012). Hippocampal place fields emerge upon single-cell manipulation of excitability during behavior. *Science, 337*(6096), 849-853. https://doi.org/10.1126/science.1221489

Lee, H., Wang, C., Deshmukh, S. S., & Knierim, J. J. (2015). Neural Population Evidence of Functional Heterogeneity along the CA3 Transverse Axis: Pattern Completion versus Pattern Separation. *Neuron, 87*(5), 1093-1105. https://doi.org/10.1016/j.neuron.2015.07.012

Lee, I., Yoganarasimha, D., Rao, G., & Knierim, J. J. (2004). Comparison of population coherence of place cells in hippocampal subfields CA1 and CA3. *Nature, 430*(6998), 456-459. https://doi.org/10.1038/nature02739

Lee, S. H., Marchionni, I., Bezaire, M., Varga, C., Danielson, N., Lovett-Barron, M., Losonczy, A., & Soltesz, I. (2014). Parvalbumin-positive basket cells differentiate among hippocampal pyramidal cells. *Neuron, 82*(5), 1129-1144. https://doi.org/10.1016/j.neuron.2014.03.034

Lein, E. S., Callaway, E. M., Albright, T. D., & Gage, F. H. (2005). Redefining the boundaries of the hippocampal CA2 subfield in the mouse using gene expression and 3-dimensional reconstruction. *J Comp Neurol*, *485*(1), 1-10. https://doi.org/10.1002/cne.20426

Leutgeb, J. K., Leutgeb, S., Moser, M. B., & Moser, E. I. (2007). Pattern separation in the dentate gyrus and CA3 of the hippocampus. *Science*, *315*(5814), 961-966. https://doi.org/10.1126/science.1135801

Leutgeb, S., Leutgeb, J. K., Barnes, C. A., Moser, E. I., McNaughton, B. L., & Moser, M. B. (2005). Independent codes for spatial and episodic memory in hippocampal neuronal ensembles. *Science*, *309*(5734), 619-623. https://doi.org/10.1126/science.1114037

Li, X. G., Somogyi, P., Ylinen, A., & Buzsaki, G. (1994). The hippocampal CA3 network: an in vivo intracellular labeling study. *J Comp Neurol*, *339*(2), 181-208. https://doi.org/10.1002/cne.903390204

Li, Y., Xu, J., Liu, Y., Zhu, J., Liu, N., Zeng, W., Huang, N., Rasch, M. J., Jiang, H., Gu, X., Li, X., Luo, M., Li, C., Teng, J., Chen, J., Zeng, S., Lin, L., & Zhang, X. (2017). A distinct entorhinal cortex to hippocampal CA1 direct circuit for olfactory associative learning. *Nat Neurosci*, *20*(4), 559-570. https://doi.org/10.1038/nn.4517

Lisman, J. E. (1997). Bursts as a unit of neural information: making unreliable synapses reliable. *Trends Neurosci*, *20*(1), 38-43. https://doi.org/10.1016/S0166-2236(96)10070-9

Lu, L., Igarashi, K. M., Witter, M. P., Moser, E. I., & Moser, M. B. (2015). Topography of Place Maps along the CA3-to-CA2 Axis of the Hippocampus. *Neuron*, *87*(5), 1078-1092. https://doi.org/10.1016/j.neuron.2015.07.007

Mankin, E. A., Diehl, G. W., Sparks, F. T., Leutgeb, S., & Leutgeb, J. K. (2015). Hippocampal CA2 activity patterns change over time to a larger extent than between spatial contexts. *Neuron*, *85*(1), 190-201. https://doi.org/10.1016/j.neuron.2014.12.001

Markus, E. J., Barnes, C. A., McNaughton, B. L., Gladden, V. L., & Skaggs, W. E. (1994). Spatial information content and reliability of hippocampal CA1 neurons: effects of visual input. *Hippocampus*, *4*(4), 410-421. https://doi.org/10.1002/hipo.450040404

Marr, D. (1969). A theory of cerebellar cortex. *J Physiol*, *202*(2), 437-470. https://doi.org/10.1113/jphysiol.1969.sp008820

Marrone, D. F., Satvat, E., Odintsova, I. V., & Gheidi, A. (2014). Dissociation of spatial

representations within hippocampal region CA3. *Hippocampus*, *24*(12), 1417-1420. https://doi.org/10.1002/hipo.22367

Masurkar, A. V., Srinivas, K. V., Brann, D. H., Warren, R., Lowes, D. C., & Siegelbaum, S. A. (2017). Medial and Lateral Entorhinal Cortex Differentially Excite Deep versus Superficial CA1 Pyramidal Neurons. *Cell Rep*, *18*(1), 148-160. https://doi.org/10.1016/j.celrep.2016.12.012

Masurkar, A. V., Tian, C., Warren, R., Reyes, I., Lowes, D. C., Brann, D. H., & Siegelbaum, S. A. (2020). Postsynaptic integrative properties of dorsal CA1 pyramidal neuron subpopulations. *J Neurophysiol*, *123*(3), 980-992. https://doi.org/10.1152/jn.00397.2019

Mizuseki, K., Diba, K., Pastalkova, E., & Buzsaki, G. (2011). Hippocampal CA1 pyramidal cells form functionally distinct sublayers. *Nat Neurosci*, *14*(9), 1174-1181. https://doi.org/10.1038/nn.2894

Nakamura, N. H., Flasbeck, V., Maingret, N., Kitsukawa, T., & Sauvage, M. M. (2013). Proximodistal segregation of nonspatial information in CA3: preferential recruitment of a proximal CA3-distal CA1 network in nonspatial recognition memory. *J Neurosci*, *33*(28), 11506-11514. https://doi.org/10.1523/JNEUROSCI.4480-12.2013

Neunuebel, J. P., & Knierim, J. J. (2012). Spatial firing correlates of physiologically distinct cell types of the rat dentate gyrus. *J Neurosci*, *32*(11), 3848-3858. https://doi.org/10.1523/JNEUROSCI.6038-11.2012

Nigro, M. J., Hashikawa-Yamasaki, Y., & Rudy, B. (2018). Diversity and Connectivity of Layer 5 Somatostatin-Expressing Interneurons in the Mouse Barrel Cortex. *J Neurosci*, *38*(7), 1622-1633. https://doi.org/10.1523/JNEUROSCI.2415-17.2017

O'Keefe, J., & Dostrovsky, J. (1971). The hippocampus as a spatial map. Preliminary evidence from unit activity in the freely-moving rat. *Brain Res*, *34*(1), 171-175. https://doi.org/10.1016/0006-8993(71)90358-1

O'keefe, J., & Nadel, L. (1979). Précis of O'Keefe & Nadel's The hippocampus as a cognitive map. *Behavioral and Brain Sciences*, *2*(4), 487-494.

Oliva, A., Fernandez-Ruiz, A., Buzsaki, G., & Berenyi, A. (2016). Spatial coding and physiological properties of hippocampal neurons in the Cornu Ammonis subregions. *Hippocampus*, *26*(12), 1593-1607. https://doi.org/10.1002/hipo.22659

Oliva, A., Fernandez-Ruiz, A., Leroy, F., & Siegelbaum, S. A. (2020). Hippocampal CA2 sharp-wave ripples reactivate and promote social memory. *Nature*,

587(7833), 264-269. https://doi.org/10.1038/s41586-020-2758-y

Orbach, J., Milner, B., & Rasmussen, T. (1960). Learning and retention in monkeys after amygdala-hippocampus resection. *Archives of neurology*, *3*(3), 230-251.

Pinault, D. (1994). Golgi-like labeling of a single neuron recorded extracellularly. *Neuroscience letters*, *170*(2), 255-260.

Pinault, D. (1996). A novel single-cell staining procedure performed in vivo under electrophysiological control: morpho-functional features of juxtacellularly labeled thalamic cells and other central neurons with biocytin or Neurobiotin. *Journal of neuroscience methods*, *65*(2), 113-136.

Preston-Ferrer, P., Coletta, S., Frey, M., & Burgalossi, A. (2016). Anatomical organization of presubicular head-direction circuits. *Elife*, *5*. https://doi.org/10.7554/eLife.14592

Ranck Jr, J. B. (1973). Studies on single neurons in dorsal hippocampal formation and septum in unrestrained rats: Part I. Behavioral correlates and firing repertoires. *Experimental neurology*, *41*(2), 462-531.

Raus Balind, S., Mago, A., Ahmadi, M., Kis, N., Varga-Nemeth, Z., Lorincz, A., & Makara, J. K. (2019). Diverse synaptic and dendritic mechanisms of complex spike burst generation in hippocampal CA3 pyramidal cells. *Nat Commun*, *10*(1), 1859. https://doi.org/10.1038/s41467-019-09767-w

Ray, S., Naumann, R., Burgalossi, A., Tang, Q., Schmidt, H., & Brecht, M. (2014). Grid-layout and theta-modulation of layer 2 pyramidal neurons in medial entorhinal cortex. *Science*, *343*(6173), 891-896. https://doi.org/10.1126/science.1243028

Roux, L., Stark, E., Sjulson, L., & Buzsáki, G. (2014). In vivo optogenetic identification and manipulation of GABAergic interneuron subtypes. *Current opinion in neurobiology*, *26*, 88-95.

San Antonio, A., Liban, K., Ikrar, T., Tsyganovskiy, E., & Xu, X. (2014). Distinct physiological and developmental properties of hippocampal CA2 subfield revealed by using anti-Purkinje cell protein 4 (PCP4) immunostaining. *J Comp Neurol*, *522*(6), 1333-1354. https://doi.org/10.1002/cne.23486

Schultz, S., Panzeri, S., Treves, A., & Rolls, E. T. (1997). Analogue resolution in a model of the Schaffer collaterals. In W. Gerstner, A. Germond, M. Hasler, & J.-D. Nicoud, *Artificial Neural Networks — ICANN'97* Berlin, Heidelberg.

Sharif, F., Tayebi, B., Buzsaki, G., Royer, S., & Fernandez-Ruiz, A. (2021). Subcircuits of Deep and Superficial CA1 Place Cells Support Efficient Spatial Coding

across Heterogeneous Environments. *Neuron*, *109*(2), 363-376 e366. https://doi.org/10.1016/j.neuron.2020.10.034

Sik, A., Penttonen, M., Ylinen, A., & Buzsaki, G. (1995). Hippocampal CA1 interneurons: an in vivo intracellular labeling study. *J Neurosci*, *15*(10), 6651-6665. https://doi.org/10.1523/JNEUROSCI.15-10-06651.1995

Slomianka, L., Amrein, I., Knuesel, I., Sorensen, J. C., & Wolfer, D. P. (2011). Hippocampal pyramidal cells: the reemergence of cortical lamination. *Brain Struct Funct*, *216*(4), 301-317. https://doi.org/10.1007/s00429-011-0322-0

Stark, E., Koos, T., & Buzsaki, G. (2012). Diode probes for spatiotemporal optical control of multiple neurons in freely moving animals. J Neurophysiol, 108(1), 349-363. https://doi.org/10.1152/jn.00153.2012

Sun, Q., Jiang, Y. Q., & Lu, M. C. (2020). Topographic heterogeneity of intrinsic excitability in mouse hippocampal CA3 pyramidal neurons. *J Neurophysiol*, *124*(4), 1270-1284. https://doi.org/10.1152/jn.00147.2020

Sun, Q., Sotayo, A., Cazzulino, A. S., Snyder, A. M., Denny, C. A., & Siegelbaum, S. A. (2017). Proximodistal Heterogeneity of Hippocampal CA3 Pyramidal Neuron Intrinsic Properties, Connectivity, and Reactivation during Memory Recall. *Neuron*, *95*(3), 656-672 e653. https://doi.org/10.1016/j.neuron.2017.07.012

Swanson, L. W., & Hahn, J. D. (2020). A qualitative solution with quantitative potential for the mouse hippocampal cortex flatmap problem. *Proc Natl Acad Sci U S A*, *117*(6), 3220-3231. https://doi.org/10.1073/pnas.1918907117

Szabo, V., Ventalon, C., De Sars, V., Bradley, J., & Emiliani, V. (2014). Spatially selective holographic photoactivation and functional fluorescence imaging in freely behaving mice with a fiberscope. *Neuron*, *84*(6), 1157-1169. https://doi.org/10.1016/j.neuron.2014.11.005

Tang, Q., Burgalossi, A., Ebbesen, C. L., Ray, S., Naumann, R., Schmidt, H., Spicher, D., & Brecht, M. (2014). Pyramidal and stellate cell specificity of grid and border representations in layer 2 of medial entorhinal cortex. *Neuron*, *84*(6), 1191-1197. https://doi.org/10.1016/j.neuron.2014.11.009

Treves, A., & Rolls, E. T. (1992). Computational constraints suggest the need for two distinct input systems to the hippocampal CA3 network. *Hippocampus*, *2*(2), 189-199. https://doi.org/10.1002/hipo.450020209

Turner, D. A., Li, X. G., Pyapali, G. K., Ylinen, A., & Buzsaki, G. (1995). Morphometric and electrical properties of reconstructed hippocampal CA3 neurons recorded in vivo. *J Comp Neurol*, *356*(4), 580-594.

https://doi.org/10.1002/cne.903560408

Vanderwolf, C. H. (1969). Hippocampal electrical activity and voluntary movement in the rat. *Electroencephalogr Clin Neurophysiol*, *26*(4), 407-418. https://doi.org/10.1016/0013-4694(69)90092-3

Wills, T. J., Lever, C., Cacucci, F., Burgess, N., & O'Keefe, J. (2005). Attractor dynamics in the hippocampal representation of the local environment. *Science*, *308*(5723), 873-876. https://doi.org/10.1126/science.1108905

Wintzer, M. E., Boehringer, R., Polygalov, D., & McHugh, T. J. (2014). The hippocampal CA2 ensemble is sensitive to contextual change. *J Neurosci*, *34*(8), 3056-3066. https://doi.org/10.1523/JNEUROSCI.2563-13.2014

Wood, E. R., Dudchenko, P. A., Robitsek, R. J., & Eichenbaum, H. (2000). Hippocampal neurons encode information about different types of memory episodes occurring in the same location. *Neuron*, *27*(3), 623-633. https://doi.org/10.1016/s0896-6273(00)00071-4

Yartsev, M. M., Witter, M. P., & Ulanovsky, N. (2011). Grid cells without theta oscillations in the entorhinal cortex of bats. *Nature*, *479*(7371), 103-107. https://doi.org/10.1038/nature10583

Zong, W., Obenhaus, H. A., Skytoen, E. R., Eneqvist, H., de Jong, N. L., Vale, R., Jorge, M. R., Moser, M. B., & Moser, E. I. (2022). Large-scale two-photon calcium imaging in freely moving mice. *Cell*, *185*(7), 1240-1256 e1230. https://doi.org/10.1016/j.cell.2022.02.017

Zong, W., Wu, R., Li, M., Hu, Y., Li, Y., Li, J., Rong, H., Wu, H., Xu, Y., Lu, Y., Jia, H., Fan, M., Zhou, Z., Zhang, Y., Wang, A., Chen, L., & Cheng, H. (2017). Fast high-resolution miniature two-photon microscopy for brain imaging in freely behaving mice. *Nat Methods*, *14*(7), 713-719. https://doi.org/10.1038/nmeth.4305

Statement of contributions

In the presented study, results were published in the following papers. Individual contributions of authors are listed as follows.

1. **Ding L, Chen H, Diamantaki M, Coletta S, Preston-Ferrer P, Burgalossi A. 2020. Structural Correlates of CA2 and CA3 pyramidal cell activity in freely-moving mice.** ***J Neurosci***

   I performed the awake, freely-moving experiments, reconstructed neuronal morphology, and analyzed electrophysiological and morphological data. I contributed to all figures of the paper. Chen helped with statistical analysis and data visualization. Diamantaki and Coletta helped with freely-moving experiments. Preston-Ferrer helped with morphological data analysis. Preston-Ferrer and Burgalossi designed and supervised the study. Burgalossi wrote the original manuscript. All authors revised and edited the manuscript.

2. **Ding L, Balsamo G, Chen H, Blanco-Hernandez E, Zouridis I, Naumann R, Preston-Ferrer P, Burgalossi A. 2022. Juxtacellular opto-tagging of hippocampal CA1 neurons in freely moving mice.** ***Elife***

   I performed opto-tagging experiments and data analysis. I contributed to all figures of the paper. Balsamo helped with the establishment of juxtacellular opto-tagging protocols. Chen and Blanco-Hernandez helped with statistical analysis and data visualization. Zouridis and Naumann gcontributed to the experiments. Preston-Ferrer and Burgalossi designed and supervised the study. Burgalossi wrote the original manuscript. All authors revised and edited the manuscript.

3. **Hodapp A[#], Kaiser ME[#], Thome C, Ding L, Rozov A, Klumpp M, Stevens N, Stingl M, Sackmann T, Lehmann N, Draguhn A, Burgalossi A, Engelhardt M, Both M. 2022. Dendritic axon origin enables information gating by perisomatic inhibition in pyramidal neurons.** ***Science***

I performed the juxtacellular recordings in awake animals and contributed to Figure 1 of the paper. Hodapp, Kaiser, Klumpp, Rozov, Stingl and Both performed experiments. Hodapp, Kaiser, Thome, Engelhardt, Rozov, Stevens, Lehmann, Sackmann and Both analyzed the data. Engelhardt Both Burgalossi and Draguhn conceived of and designed the experiments. Both and Draguhn wrote the original manuscript. All authors revised and edited the manuscript.

Acknowledgements

First of all, I would like to thank my supervisor Prof. Andrea Burgalossi for his advice, support and insightful guidance during my whole Ph.D. time. I would also like to thank my advisory board member Prof. Olga Garaschuk and Prof. Jan Benda, for their comments and valuable suggestions for my projects.

Then I would like to thank my colleagues and collaborators, not only for their assistance and contributions to the projects, but also for their company on the journey.

I would like offer my special thanks to my partner, friends and family. Without their understanding and encouragement, it would be impossible for me to complete my study.